Climate change is driving unprecedented European ocean temperatures, with severe impacts for marine life

Authors

Claire Bergin, *ICARUS Climate Research Centre, Maynooth University, Maynooth, Ireland*
Ben Clarke, *Centre for Environmental Policy, Imperial College, London, UK*
Clair Barnes, *Centre for Environmental Policy, Imperial College, London, UK*
Catherine Gregory, *Climate and Environmental Physics, Physics Institute, University of Bern, Bern, Switzerland*
Kristina Dahl, *Climate Central, Princeton, NJ 08542, USA*
Brandon Bouassa, *Climate Central, Princeton, NJ 08542, USA*
Thomas Frölicher, *Climate and Environmental Physics, Physics Institute, University of Bern, Bern, Switzerland*
John Bruno, *The University of North Carolina at Chapel Hill, Chapel Hill, North Carolina, USA*
Maja Vahlberg, *Red Cross Red Crescent Climate Centre, The Hague, the Netherlands; Swedish Red Cross, Stockholm, Sweden (based in Ubmeje/Umeå, Sweden)*
Ana Meija, *Red Cross Red Crescent Climate Centre, The Hague, The Netherlands (based in Ecuador)*
Chris Boyer, *Red Cross Red Crescent Climate Centre, The Hague, The Netherlands (based in Washington, USA)*
Friederike Otto, *Centre for Environmental Policy, Imperial College, London, UK*

Review authors

Theodore Keeping, *Centre for Environmental Policy, Imperial College, London, UK*
Izidine Pinto, *Royal Netherlands Meteorological Institute (KNMI), De Bilt, The Netherlands*
Peter Thorne, *ICARUS Climate Research Centre, Maynooth University, Maynooth, Ireland*
Roop Singh, *Red Cross Red Crescent Climate Centre, The Hague, The Netherlands (based in New Jersey, USA)*

Cite as Bergin, C. et al. (2026): Climate change is driving unprecedented European ocean temperatures, with severe impacts for marine life (WWA scientific report No. 90) World Weather Attribution. DOI:10.25560/132103

Main findings

- Extremely high SSTs and marine heatwaves have disastrous consequences for marine ecosystems, leading to mass mortality events of habitat forming species such as corals, sponges and macroalgae. The loss of such foundation species impacts the structure and function of the entire ecosystem. Mass mortality events caused by extreme heat can thus lead to mass mortality events further down the food chain for invertebrates, fish, seabirds and marine mammals.
- Marine heatwaves can make local conditions increasingly unsuitable for marine species adapted to historical temperatures, driving species range shift, changes in community composition and the replacement of species by more warm-adapted organisms. These impacts can be particularly pronounced for benthic and demersal species, which have limited ability to move to more suitable temperatures, making seafloor ecosystems especially vulnerable to warming and heat extremes.
- The impacts are not exclusively ecological. Global research has shown that high SSTs can influence regional climate phenomena, including monsoon rainfall, and can interact with tropical cyclones, potentially making them more destructive. For Europe, high Mediterranean temperatures have, for example, been linked to the extreme rainfall events such as the Valencia floods in 2024.
- When assessing observational datasets of SSTs, we find that this year's event is not a rare event in today's climate, in which the planet has warmed by 1.4°C, with return periods ranging from approximately 1 year in the Eastern Mediterranean to 5 years in the Western Mediterranean for the annual warmest 14-day period (SST14x) event.
- For the warmest 14-day period (SST14x) July events, the return times are quite different between different datasets, and in some of them much rarer than the annual event, with a return period of up to 90 years in the Bay of Biscay and Iberian Peninsula (BIP) region.
- As expected, there are strong trends in SSTs across all four regions and for both temporal definitions. The Celtic region shows the smallest change, with temperatures increasing by 1.2°C. The probability ratio is approximately 30, suggesting that this would have been a roughly 1-in-100-year event in a climate 1.4°C cooler. In the three other regions, the SST14x values observed would have been virtually impossible in a pre-industrial climate. Observations suggest that temperatures in the BIP region have increased by 1.5°C, compared with 3.1°C in the WMed and 2.6°C in the EMed. The increases in the latter two regions substantially exceed the level of global warming.
- Focusing specifically on SST14x during July, we find for all regions July exhibits the fastest rate of change compared to the annual SST14x and observations indicate that these July events would have been virtually impossible in a pre-industrial climate, while the change in intensity ranges from 1.5°C in the Celtic region and 3.4°C in the Western Mediterranean.
- We also assessed the rate of change in all calendar months, finding that the rate of change in SSTs is strongest in the summer months, and especially in the Mediterranean far exceeding global warming. The shoulder months, especially in spring, also show a warming much greater than the global average.
- To assess whether all of the observed warming is attributable to human-induced climate change, we combine observations and climate models for the annual SST14x event. We find that, in the Celtic region, climate models and observations show very similar trends, while in

all other regions the observed trends are much stronger than those simulated by climate models. Despite this, we find that in the two Mediterranean regions, the increase in warming attributable to human-induced climate change is about 2°C, substantially surpassing the level of global warming, even under this conservative estimate. BIP follows global warming very closely, with an attributable increase in intensity of 1.4°C, and a slightly smaller increase of 1.3°C in the Celtic region. In all four regions, these events would have been very rare in a 1.4°C cooler climate despite being common today.

- When analysing the same regions and events but for a 1.4°C warmer future (2.8°C since pre-industrial, the current warming level expected at the end of this century) we find the changes in intensity to continue at a similar rate, so that the events observed in 2026 would be another 1.3°C to 1.9°C hotter.
- In addition, we analyse the role of climate change in the frequency of marine heatwaves, defined as exceeding the local 90th percentile threshold from the 1982-2011 climatology for at least five days. We find that in the Celtic region 80% of the area experienced MHWs compared to only 30% in a 1.4°C cooler climate, in the BIP region the change is from only 40% to 90% today, in the Western Mediterranean the change is from 40% to 80% while in the Eastern Mediterranean only 9% of the area would have experienced heatwaves in a 1.4°C cooler climate compared to nearly 70% today.
- Our results projecting the intensity of such events in a warmer climate exhibit temperatures above what many species living in our seas today can tolerate, showing strong limits to adaptation. Thus, a rapid transition away from fossil fuels is essential to save crucial ecosystems, fisheries, food production and tourism along the European coasts.
- Adaptation to increasing marine temperatures can increase resilience and reduce vulnerability, but cannot fully offset the ecological impacts of continued ocean warming. Adaptation measures can include reducing additional pressures on marine ecosystems, protecting habitats, adapting fisheries and aquaculture management, and improving monitoring and early-warning systems.

1 Introduction

Over the past few decades Sea Surface Temperatures (SSTs) have been rising globally, with July 2026 seeing global sea temperatures hitting their hottest July on record (The Guardian, 2026), see Fig. 1.1. Since May 2026, Europe has experienced numerous terrestrial heatwaves as well as record-breaking temperatures as a number of high-pressure systems stalled over the continent. Climate change attribution studies, such as Keeping et al. (2026), have shown that the severity of these heatwaves has been directly increased by human-caused climate change. While many attribution studies have been carried out on land-based extreme heat events globally (Zachariah et al., 2023, Antonio Rivera et al., 2023, Philip et al., 2022), there is less literature (e.g., Laufkötter et al., 2020) pertaining to the attribution of specific sea-based extreme heat events known as marine heatwaves (MHWs) despite numerous publications on the phenomena and their impacts (e.g. Capotondi et al., 2024, Garrabou et al., 2022, Oliver et al., 2021).

Across Europe, marine life is being affected by high SSTs and subsurface temperatures. For example in the UK, a major octopus bloom may be impacting other marine life (Gov.uk, 2026). More generally, the northward shift of invasive marine species' ranges to previously cooler waters is proving detrimental to native species in seas across Europe (Independent, 2026, Irish Examiner, 2026). This range shift affects not only the fish, bivalves, and crustaceans that are farmed for human consumption, but dolphins have also been spotted eating jellyfish because their normal diet of mackerel is in decline (BBC, 2026).

As people take to beaches to cool down from the land-based heatwaves, the European Centre for Disease Prevention and Control (ECDC) has warned of increased risk of water borne diseases such as Vibriosis (ECDC, 2026). In addition, a rise in jellyfish has been recorded in seas as climate change causes low-oxygen zones, where jellyfish thrive over other fish, this directly affects tourism as beach closures are issued (Calbert, 2025). In Spain, rising temperatures provide homes for invasive seaweed which is blanketing many Spanish beaches, making them less attractive in tourist season (Laamraoui et al., 2024).

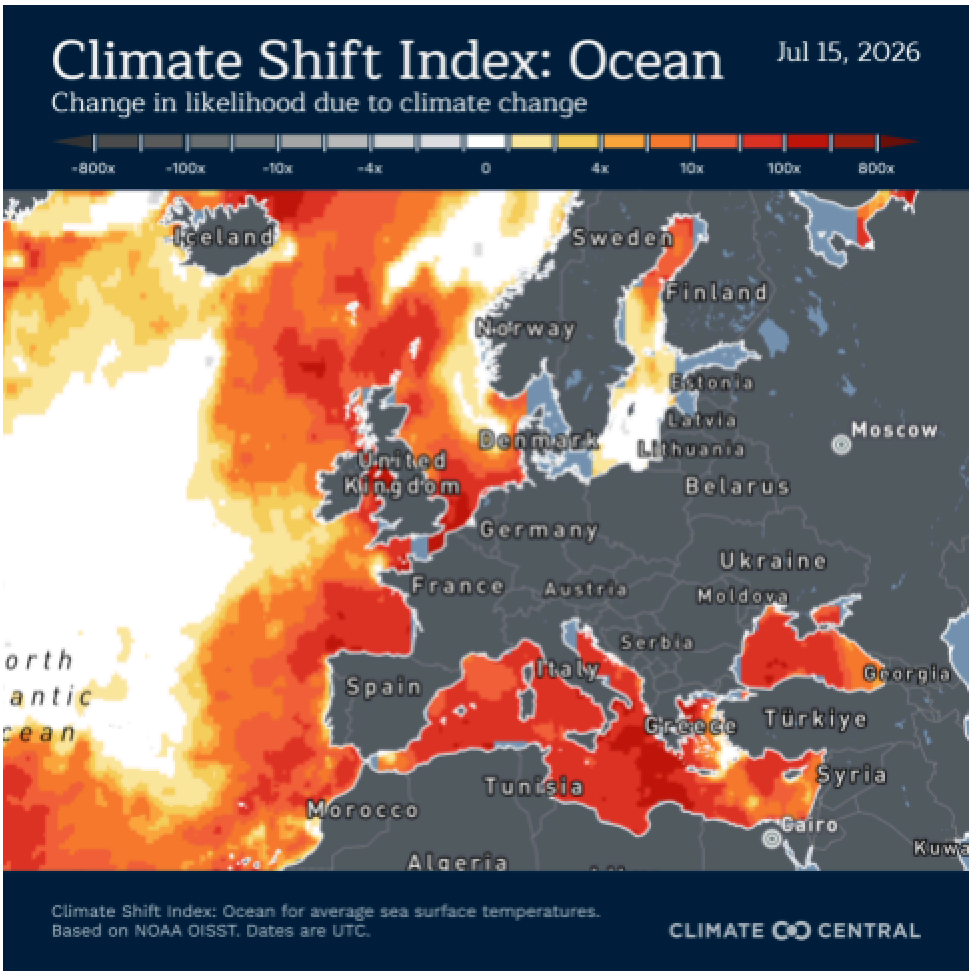

Figure 1.1: *The climate shift index for the 15th July 2026. Showing the change in likelihood of sea surface temperatures on the colour bar from -1000 to 1000, where positive numbers are more likely due to climate change (negative scores indicate temperatures that are less likely). Data and images obtained from Climate Central.*

The effects of MHWs are not limited to the ocean. The Monin–Obukhov similarity theory relationship means warmer SSTs lead to a similar magnitude of warmer marine air temperatures on climate timescales (Casasanta et al., 2025). The well known Clausius-Clapeyron relationship means that for every 1°C increase in temperature, the atmosphere over unlimited water surfaces can hold an extra approximately 7% of water vapour. This increased air heat and humidity will have direct impacts for coastal communities via elevated night-time temperature minima and increased humidity – which can have major health impacts. However, elevated SSTs have been repeatedly linked, prior extreme precipitation event studies, as an important contributory factor through increasing the total precipitable water (Kew et al., 2025, Clarke et al., 2025, Clarke et al., 2024). In particular, marine heatwaves have been shown to act as extra fuel for the storm, making it stronger and increasing several hazards, including flooding, high waves, and storm surge, including storm Babet (Goswami et al., 2026) and the extreme rainfall event in 2024 in Valencia (Saurral et al., 2026). Thus, the high SSTs may be priming the atmosphere for extreme precipitation and flooding events later in the year.

1.1 High sea surface temperatures in Europe

In Chapter 9 of its sixth assessment report (AR6), Working group 1 of the Intergovernmental Panel on Climate Change (IPCC WG1) reported a robust warming of the world's oceans by approximately 0.88°C from 1850-1900 to 2011-2020, most of which occurred since 1980 (IPCC, 2021). Since the 1970s, over 90% of the excess heat induced by anthropogenic activities has been stored by the world's oceans, the majority of which is in the layer from the surface to a depth of 700m (Forster et al., 2026). Between 2016 and 2025, the oceans warmed at a rate of 0.27°C per decade (0.2°C - 0.4°C) (Forster et al., 2026).

MHWs, defined as sustained periods of anomalously high ocean temperatures that can lead to severe and persistent impacts on marine ecosystems, have become much more likely, more intense and longer as a result of this excess heat (Frölicher et al., 2018; IPCC, 2021). The number of days experiencing surface MHWs has more than tripled between 1991 and 2025 (Forster et al., 2026), while the most extreme and impactful events have increased more than 20-fold in frequency (Laufkötter et al., 2020). Frölicher et al. (2018) detected a doubling in MHWs between 1982-2016 and reported that, with 1°C of global warming at the time. Approximately 87% of MHWs were found to be attributable to anthropogenic warming, rising to essentially 100% at 2°C of global warming or beyond. In line with this, Giguere et al. (2024) found that, in July 2023, in excess of 70% of the ocean's temperatures on any given day were made at least twice as likely to occur because of global temperature rise. In addition, an increase of 1°C in the maximum intensity of extreme sea temperature events was found to be directly linked to human-caused climate change (Marcos et al., 2025).

Recent years have seen exceptional and record-breaking marine heat across the Mediterranean Sea. In June 2025, the Mediterranean experienced its warmest June on record, with 62% of the basin affected by strong or more intense marine heatwaves; in the western Mediterranean, daily SST reached a June record of 27.0°C, 3.7°C above the 1991–2020 average (Copernicus, 2025; Mercator Ocean International, 2025). These extremes have continued into 2026, with a buoy off Mallorca recording a water temperature of 33.02°C in August, a new record. The Mediterranean Sea is warming extremely rapidly (Pastor et al., 2019; Napolitano et al., 2025), driving a wide range of ecological impacts across the basin. According to a 2021 report by WWF, the ranges of 1,000 non-native marine species have shifted into the Mediterranean due in large part to warming. This includes aggressive predators such as lionfish, that are displacing resident species (WWF, 2021). The increasing temperatures in the Mediterranean and associated rise in MHWs have also caused recurrent mass mortality events of marine organisms, highlighting the detrimental effects of climate change to the health and functioning of marine ecosystems (Artana et al. 2026; Garrabou et al., 2022). Bonino et al. (2025) found that marine heatwaves in the Mediterranean are linked with persistent subtropical anticyclonic ridges which cause a weakening of the prevailing winds, conditions which have brought widespread hot and dry conditions in early summer 2026.

Observed SSTs have increased around European coasts in the Northeast Atlantic, with the exception of slight cooling in the subpolar region to the west due to ice melt (IPCC, 2021). In line with this, MHWs have also increased in frequency in the region (Atkins et al., 2025, Ospina et al., 2026). In early summer 2023, the northwestern European shelf and Bay of Biscay experienced substantially elevated SSTs driven by strong atmospheric forcing under persistent anticyclonic conditions (England et al., 2025). The resulting MHW subsequently fed back onto the atmosphere, reducing cloud cover over the ocean and enhancing the transport of heat and moisture over land, thereby contributing to more extreme conditions over land (Berthou et al., 2024). This event was enhanced substantially by recent rapid increases in sea surface temperatures (Berthou et al., 2024; Atkins et al., 2025) related to anthropogenic warming (England et al., 2025). Importantly, these changes are not confined to the ocean surface: Wilson et al. (2025) project that damaging seafloor heat extremes on the northwestern European shelf will increase in frequency and severity even more strongly than surface MHWs, highlighting the potential for intensifying heat extremes throughout the water column in European shelf seas.

Despite the robust connection with global climate change and widespread impacts of these events, to our knowledge, no full attribution studies (using both observations and climate model data) on elevated SSTs in the Mediterranean or Northeast Atlantic exist. This study seeks to address this gap by directly assessing the anthropogenic influence on recent periods of high SSTs in the Northeastern Atlantic and Mediterranean regions.

1.2 Event Definitions

Large areas of the seas surrounding Europe have been affected by high SSTs in spring and summer 2026. To examine the effect of human-caused climate change on these elevated SSTs we focus on four different spatial regions (Fig. 1.2):

- **Celtic**: Comprising the Irish Sea and St. George's Channel, Celtic Sea, English Channel, Bristol Channel, Inner Seas off the West Coast of Scotland, plus an extension west from these defined regions to 15°W between 48°N and 59°N.
- **Bay of Biscay and Iberian Peninsula (BIP):** Comprising the Bay of Biscay plus an extension west to 14°W between 36°N and 48°N.
- **West Mediterranean (WMed):** Comprising the Western Mediterranean Sea Basin, Alboran Sea, Balearic (Iberian Sea), Ligurian Sea and Tyrrhenian Sea.

- **East Mediterranean (EMed):** Comprising the Eastern Mediterranean Sea Basin, Adriatic Sea, Ionian Sea and Aegean Sea.

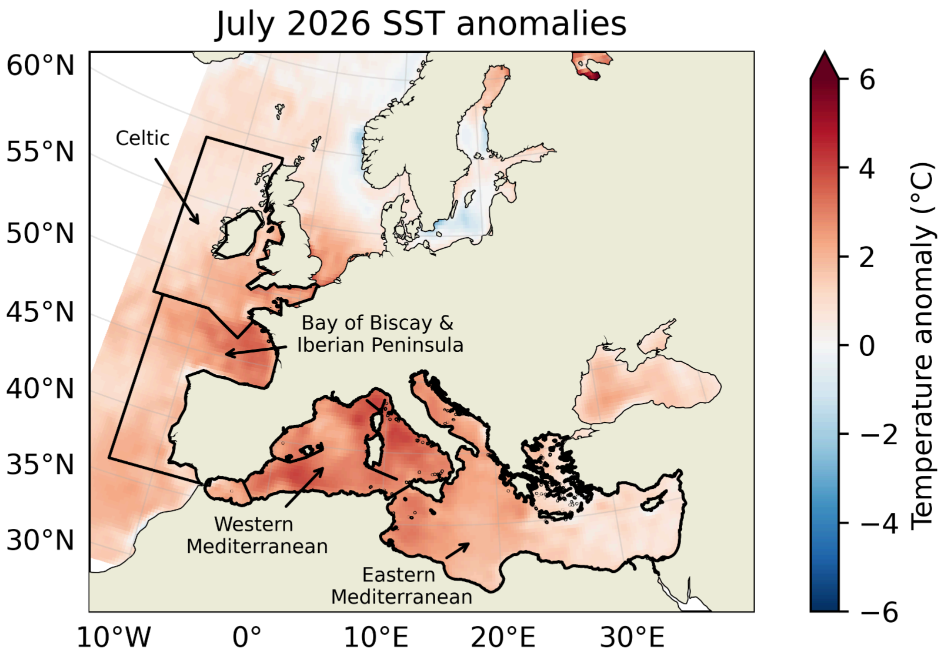

Figure 1.2: *Anomalies in July 2026 Sea Surface Temperatures around Europe with respect to 1990-2020 climatological average for July. Labelled regions with bold outlines indicate the Data: OISST NOAA.*

For all four spatial regions we consider trends in the annual maxima of 14-day sea surface temperatures (Fig. 1.3), denoted SST14x. In addition, using only observation products, we consider trends in July maxima of 14-day sea surface temperatures, denoted SST14x-July. By using both definitions for all spatial regions, we aim to assess changes in both extreme SSTs at any time of year and the comparatively early arrival of very warm temperatures in 2026. By end of July the BIP and WMed regions area-averaged SSTs reached all time records in the observational period for NOAA OISST data. In addition, the Celtic region was the third warmest on record.

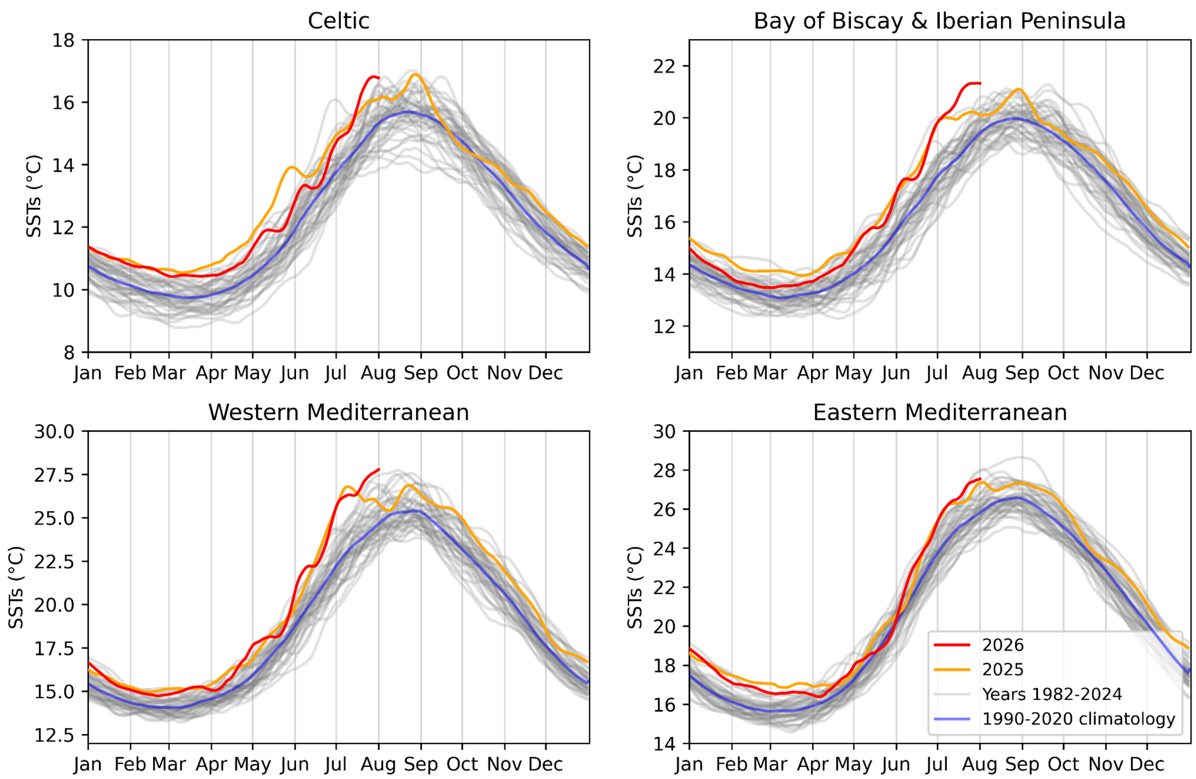

Figure 1.3: *14-day mean SSTs for each region for all years in the NOAA OISST dataset. All years are shown in grey, with the climatological mean for 1990-2020 shown in blue, 2025 temperatures in orange and 2026 in red.*

For each event definition, we study the influence of anthropogenic climate change by comparing the likelihood and intensity of similar hot SSTs at present with those in a 1.4°C cooler climate without human-caused warming (based on Forster et al., 2026). We also extend this analysis into the future by assessing the influence of a further 1.4°C of global warming from present. This is in line with the latest Emissions Gap Report from the United Nations Environment Programme, which shows that the world is on track for at least 2.8°C temperature rise given currently implemented policies (UNEP, 2025).

2 Observational analysis

The methods used to analyse heat trends follow the standard WWA protocol using non-stationary extreme value theory, as described in Philip et al. 2020 and expanded upon in Otto et al., 2024. Specifically, the extremes indices SST14x and SST14x-July in each region are modelled using a Gaussian distribution that is assumed to shift with global mean surface temperature (see Appendix A1 for details of data and methods). A GEV was also checked but the Gaussian distribution better represented the data. In this study we conduct an observation-only analysis for SST14x-July and combine observation-based gridded products and climate models for SST14x. In line with the protocol described in Philip et al. 2020, climate models are evaluated in their representation of observed weather and climate characteristics of the region (see Appendix A3).

At the time of writing in early August 2026, the SSTs around Europe remain anomalously high. Furthermore, the typical season for peak SSTs is only beginning, with sea temperatures tending to cool in Europe in September/October (Fig. 1.3). It is therefore expected that SSTs will plateau or even increase further throughout the late summer season. Nonetheless, with record-high SSTs already emerging and impacts on marine life clear throughout the study regions, analysis of the influence of human-caused climate change on this period of elevated SSTs is already pertinent.

2.1 Trends in gridded data

All gridded observation-based datasets are outlined in detail in Appendix A1.1.

2.1.1 Annual 14-day maxima

The 14-day annual maxima of SST is calculated for each observational data product in each geographical region outlined in section 1.3. The return period estimate(s) in observation-based datasets with the event included suggest that the conditions observed in July 2026 are now relatively common in all regions in the present climate, with such conditions expected approximately once every 3 years in the Celtic region, once every 5 years in BIP, once every 5 years in WMed, and two out of every three years in EMed (Table 2.1). These estimates are consistent across datasets, with substantially overlapping 95% confidence intervals. We further note that the choice of return period affects the estimated probability ratios but that the estimated changes in intensity are independent of this. The results for the influence of human-caused climate change in each of the observational datasets are also shown in Table 2.1, with both probability ratios for events of equivalent intensity, and changes in intensity of an event of equivalent likelihood. All results are discussed in detail below.

Region	Chosen return period	Dataset	Annual maximum 14-day SSTs		Change due to 1.4°C global warming	
			Event magnitude (°C)	Return period (years)	Probability ratio	Change in magnitude (°C)
Celtic	3	OISST	16.9	3.57 (2.00, 10.7)	28.0 (11.4, 2000)	1.11 (0.10, 2.03)

		ERA5	16.8	3.27 (2.09, 6.75)	44.6 (8.23, 500)	1.15 (0.68, 1.56)
		OSTIA	16.8	2.47 (1.59, 6.05)	25.45 (1.93, 1410)	1.36 (0.23, 2.01)
Biscay & Iberian Peninsula	5	OISST	21.4	4.77 (2.63, 13.79)	21300 (174, >1m)	1.65 (1.04, 2.11)
		ERA5	21.4	6.18 (3.50, 15.17)	513 (42.2, 15900)	1.27 (0.84, 1.62)
		OSTIA	21.4	3.38 (1.98, 9.86)	784 (41.5, 163000)	1.64 (0.83, 2.49)
Western Mediterranean	5	OISST	27.9	4.30 (2.19, 16.1)	>1m (60800, >1m)	3.33 (2.39, 4.11)
		ERA5	27.9	6.22 (3.15, 20.17)	24300 (1430, >1m)	2.5 (1.83, 3.1)
		OSTIA	28.0	2.65 (1.59, 7.89)	15700 (352, >1m)	3.43 (2.07, 4.76)
Eastern Mediterranean	1.5	OISST	27.6	1.23 (1.04, 1.74)	>1m (78200, >1m)	2.77 (2.03, 3.57)
		ERA5	27.5	1.39 (1.15, 1.92)	955 (160, 15800)	1.88 (1.51, 2.28)
		OSTIA	27.6	1.09 (1.01, 1.29)	32800 (1390, >1m)	3.19 (2.14, 4.43)

Table 2.1: *Observed magnitude and estimated return period of the SST14x metric in each study region and dataset. The probability ratio and change in magnitude for SST14x in each study region and dataset due to the influence of increased GMST are also shown along with 95% confidence intervals. Note: ">1m" means more than one million.*

Figures 2.1 and 2.2 show time series and statistical fits to the SST14x index calculated from the OISST data in each region, respectively. Table 2.1 further shows that, in all regions, all datasets show a strong and statistically significant warming signal. The Celtic region shows the weakest warming rate of the four study regions and the widest uncertainty range. This is likely due to the pronounced decadal-scale variability, linked to Atlantic Multidecadal Variability, a phenomenon much discussed in the literature (Qin et al., 2022, Bellomo et al., 2018, Frankignoul et al., 2017) in the SST14x time series that is not captured by the GMST covariate (Fig. 2.1a). However, with best estimates of the probability ratios at approximately 25 to 45, an event that is expected now once every 3 years would have been expected approximately only every 100 years in a preindustrial climate. In the other three regions, the statistical model is even more robust and shows stronger changes, with best estimates of the probability ratios varying from the hundreds of times more likely to more than a million times more likely. This suggests that such temperatures would have been very highly unlikely in a preindustrial climate in all cases and at any point during the summer season in any of these regions. This is despite these high SSTs occurring well in advance of what is typically the peak of the seasonal cycle in SSTs in all four regions being studied (Figure 1.3). Due to SSTs varying relatively slowly compared to air temperatures, there is a larger signal-to-noise ratio in the data. Therefore, we find that resultant probability ratios are much larger for the high SST events outlined in this report compared to air temperature or rainfall events.

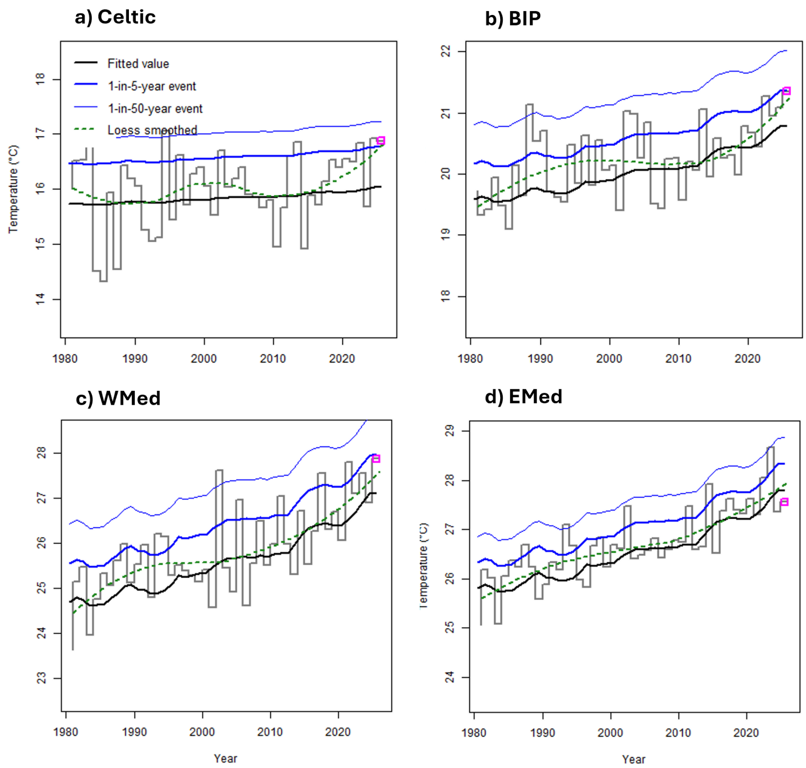

Figure 2.1: *Time series of SST14x in each study region: a) Celtic, b) BIP, c) WMed, d) EMed. The modelled influence of GMST on the expected value (6- and 40-year return period value) is shown with the black line (blue, bold blue lines), while the loess smoothed trend is shown with the green dashed line. The pink box shows the magnitude of the observed event.*

Underlying these changes, the absolute warming rate in the SST14x index varies between regions. The most extreme temperatures in the Celtic region have warmed by approximately 1.2°C, slightly below the average global warming rate. Similarly, extremes in the BIP region to the south have warmed by approximately 1.5°C when averaging across datasets, comparable to the global warming rate and above the average temperature rise of the ocean. The Mediterranean regions are warming fastest, with approximately 3.1°C in the west and 2.6°C in the east, far more rapidly than the global mean. It is noteworthy that the shorter datasets, OISST and OSTIA which begin in the 1980s, give consistently stronger warming rates with respect to global warming than ERA5, which begins in 1940 - this likely reflects more rapid warming over recent decades. However, this period also represents greatly improved data coverage and consistency due to the inclusion of satellite-based remote sensing, which is especially of value over large bodies of water. We therefore combine all datasets in our synthesis.

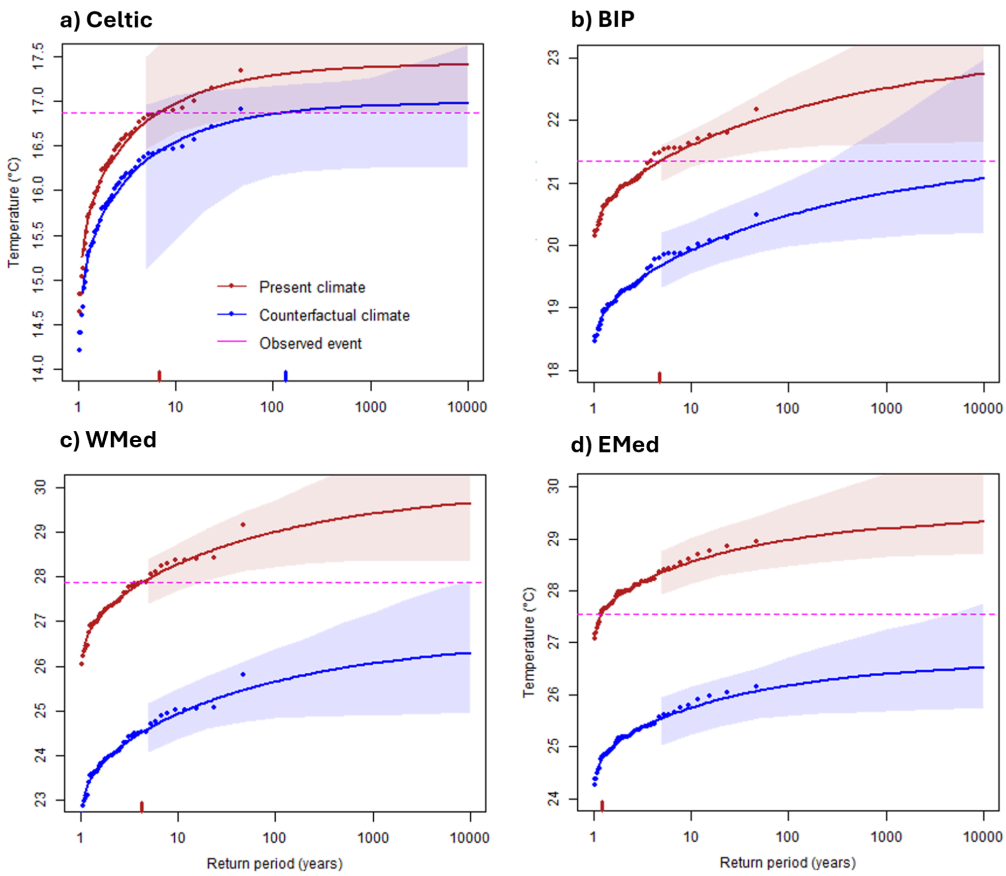

Figure 2.2: *Statistical fits to SST14x from OISST in each study region: a) Celtic, b) BIP, c) WMed, d) EMed. The influence of the current GMST conditions is shown with the red vs blue probability curves, showing the present vs preindustrial warming levels. The magnitude of the 2026 event is highlighted with a horizontal purple line.*

2.1.2 July 14-day maxima

By limiting the 14-day maxima to July only, we better estimate the likelihood of such early hot periods in each region in the current climate, as well as how earlier season heat is changing with respect to the wider summer season as the world warms. As expected, the conditions observed in July 2026 are less likely to occur in July than over the full year, especially further into the warm water season (August - September) across all regions. Though the absolute likelihood varies more strongly by region: such conditions are now expected in July approximately once every 10 years in the Celtic region, a wide range of estimates from 20-90 years in BIP, 3 years in EMed, and 15 years in WMed (Table 2.2). These estimates are also less consistent across datasets than in the annual index, partially reflecting the smaller sample size. The results for the influence of human-caused climate change in each of the observational datasets are also shown in Table 2.2, with both probability ratios for events of equivalent intensity, and changes in intensity of an event of equivalent likelihood. All results are discussed in detail below.

Region	Dataset	Annual maximum 14-day SSTs		Change due to 1.4°C global warming	
		Event magnitude (°C)	Return period (years)	Probability ratio	Change in magnitude (°C)
Celtic	OISST	16.8	9.00 (3.51, 53.1)	1020 (15.2, >1m)	1.53 (0.60, 2.42)
	ERA5	16.8	13.9 (5.51, 71.5)	3690 (199, 204000)	1.39 (0.92, 1.83)
	OSTIA	16.8	5.97 (2.61, 28.2)	881 (18.4, 539000)	1.56 (0.66, 2.45)
Bay of Biscay & Iberian Peninsula	OISST	21.3	40.2 (10.2, 1040)	889000 (1320, >1m)	1.87 (1.12, 2.59)
	ERA5	21.4	91.0 (18.6, 850)	24400 (748, >1m)	1.41 (0.94, 1.88)
	OSTIA	21.3	20.4 (5.95, 208)	98700 (362, >1m)	1.82 (1.03, 2.62)
Western Mediterranean	OISST	27.7	11.6 (4.22, 202)	>1m (29300, >1m)	3.77 (2.40, 4.92)
	ERA5	27.9	23.8 (7.63, 175)	16100 (1080, >1m)	2.61 (1.79, 3.38)
	OSTIA	27.7	5.04 (2.34, 28.3)	>1m (11900, >1m)	3.93 (2.42, 5.11)
Eastern Mediterranean	OISST	27.5	2.58 (1.52, 8.27)	>1m (>1m, >1m)	3.24 (2.46, 3.98)
	ERA5	27.5	4.43 (2.33, 12.5)	58400 (4740, >1m)	2.00 (1.54, 2.45)
	OSTIA	27.5	1.41 (1.10, 2.29)	>1m (>1m, >1m)	3.56 (2.80, 4.31)

Table 2.2: *As in Table 2.1 but for the SST14x-July metrics.*

Figures 2.3 and 2.4 show time series and statistical fits to the SST14x-July index calculated from the OISST data in each region, respectively. Table 2.2 further shows that, in all regions in July, as in the annual index, all datasets show a strong and statistically significant warming signal. Furthermore, the warming rate in July is consistently higher than the annual peak. The Celtic, BIP and Wmed regions all experienced record warm temperatures using this metric in 2026 and the EMed region experienced its 3rd warmest annual record, surpassed by 2023 and 2024. The record warmth was particularly stark in the BIP region surpassing the previous record by about 0.5℃

The Celtic region again has the weakest warming rate of the study regions, though the decadal-scale variability in the SST14x time series is not present and the trend is better captured by the statistical model through the GMST covariate (Fig. 2.3a). For July, all best estimates of the probability ratios are close to or in excess of 1000 (Fig. 2.4), suggesting that observing such temperatures in July would have been virtually impossible in a preindustrial climate in any of the study regions. The absolute warming rate in July extremes mirrors the changes observed annually, with variation between regions. The most extreme temperatures in the Celtic region have warmed by approximately 1.5°C and the BIP region by 1.7°C, similar to the average global warming rate and above the average temperature rise of the oceans. The Mediterranean regions are warming even faster, with approximately 2.9°C in the east and 3.4°C in the west, more than double the global warming rate and more than triple the global ocean warming rate.

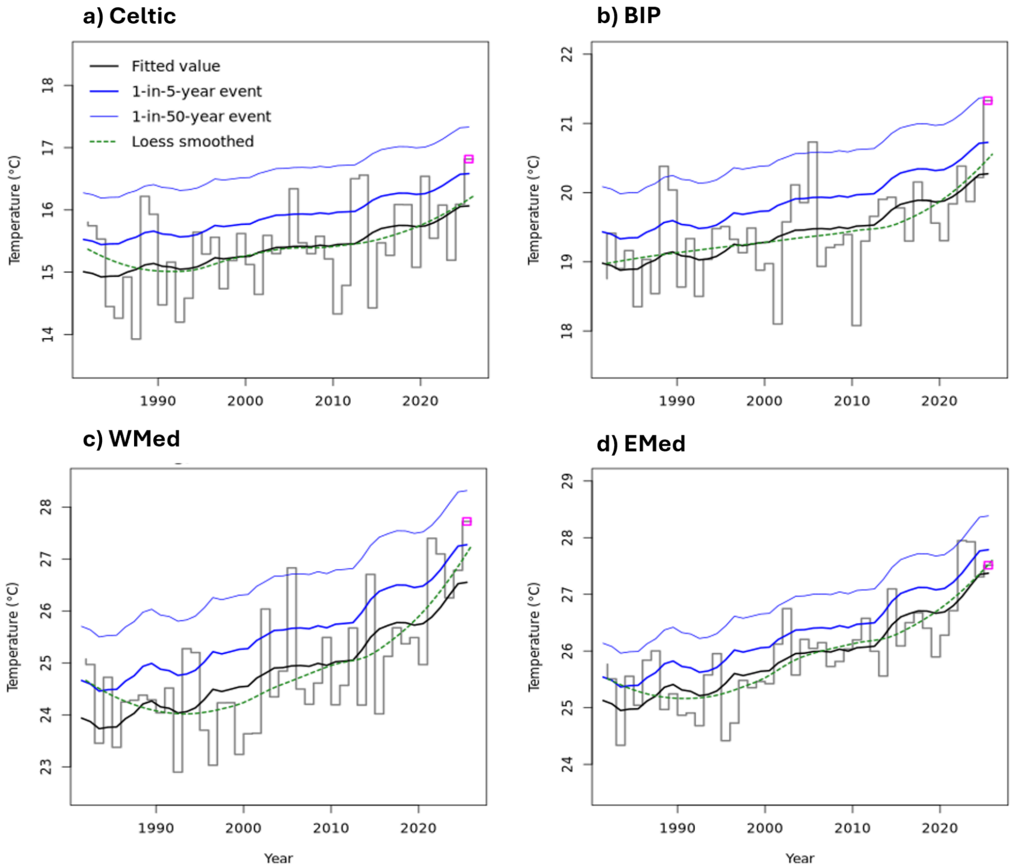

Figure 2.3: *As in Figure 2.1 but for the SST14x-July metrics.*

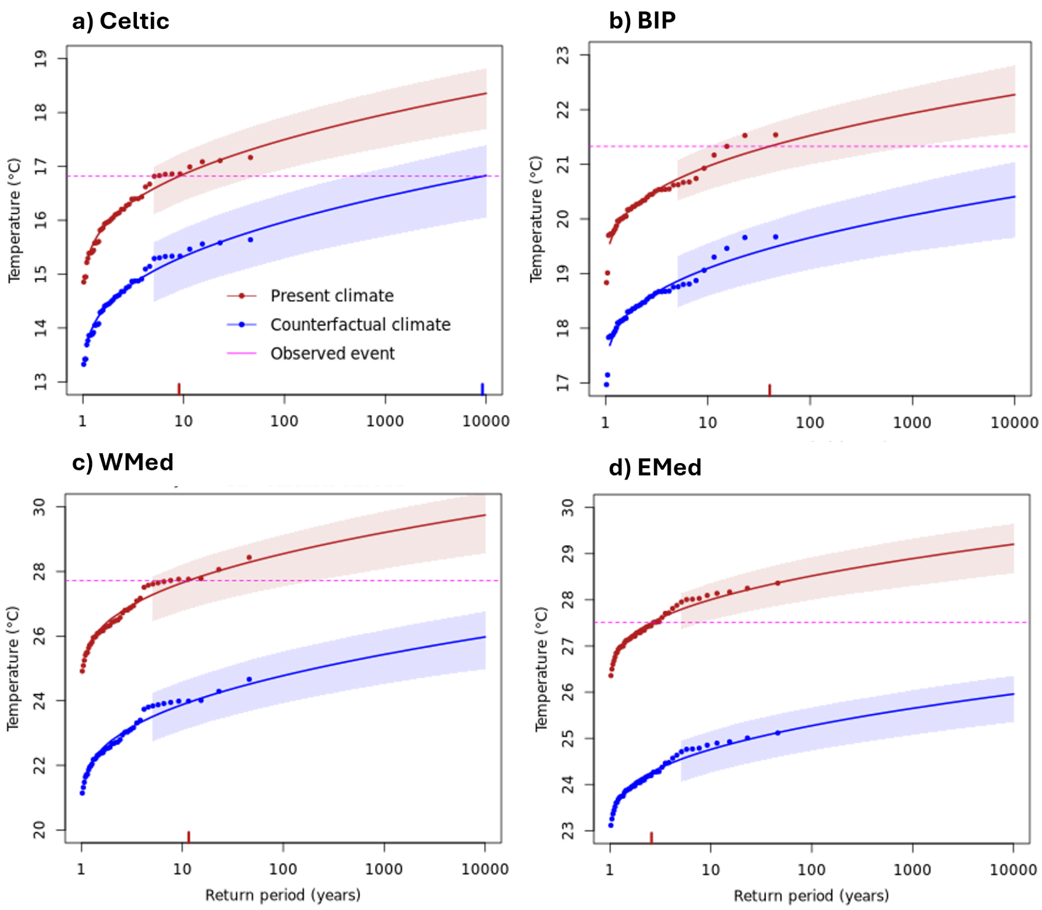

Figure 2.4: *As in Figure 2.2 but for the SST14x-July metrics.*

2.2 Change per calendar month

To further explore changes in SSTs at different times of year, we calculate the change in monthly mean temperatures per degree of global mean surface temperature rise (Fig. 2.5, Fig. A2.1) using ERA5, OISST, and two additional longer monthly-only resolution datasets (HadISST and ERSST - see Appendix A1.1). These charts reflect and reinforce several of the general findings in section 2.1: all regions are warming at a rate at or exceeding the rise in global mean surface temperatures (and therefore above the rate of globally averaged SST rise), the two Mediterranean regions are warming faster than those in the North Atlantic, the early summer (June and July) are warming faster than other parts of the summer and especially in the Mediterranean regions. The charts further show that summer temperatures as a whole are warming faster than in winter, and that the shoulder seasons (May - June and September - November) are warming at the fastest rates, particularly in the BIP region.

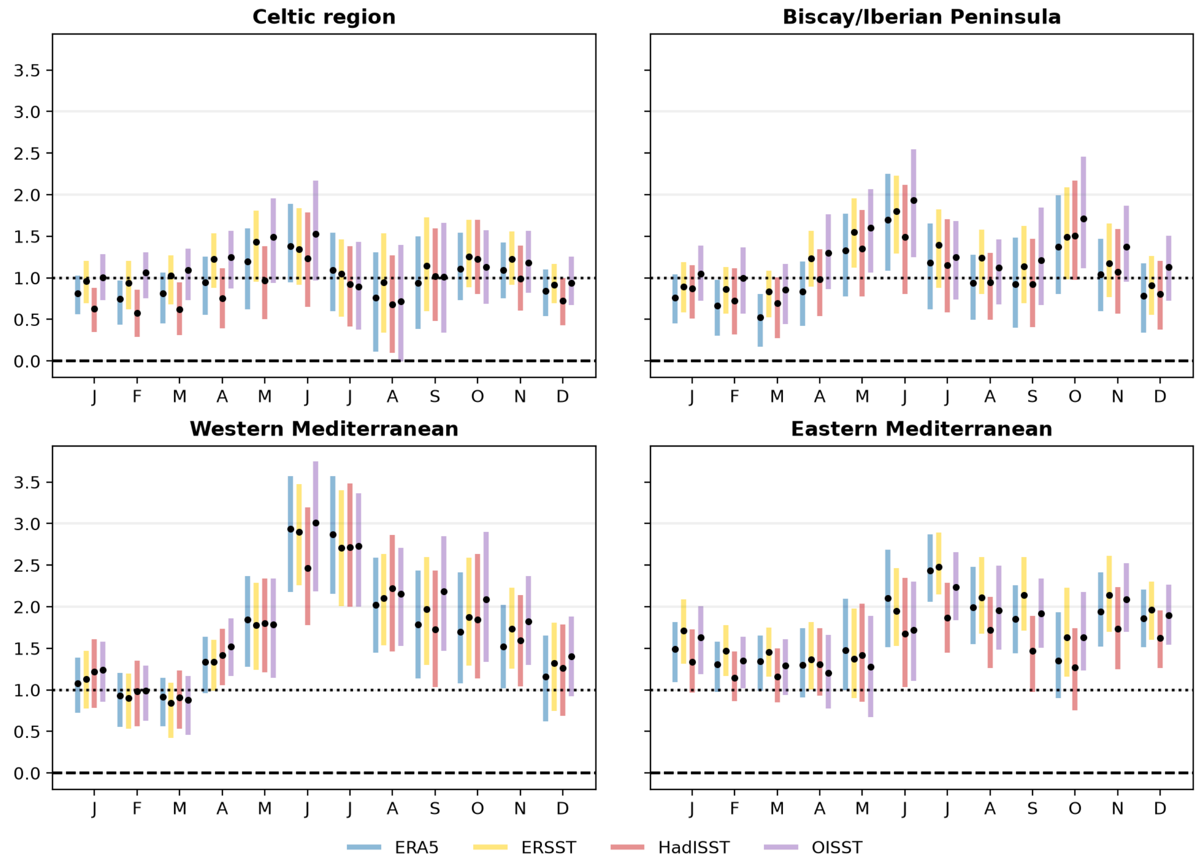

Figure 2.5: *Change in monthly mean temperature per degree of global mean surface temperature from 1980-2026 in the four study regions, from four observational datasets: ERA5, ERSST, HadISST, OISST (see Appendix A1.1). Values above the dotted line indicate that the region has warmed more than the planet as a whole over the same period.*

2.3 Changes in MHWs

We consider extreme occurrences of SSTs by examining marine heatwaves (MHWs). Here, we define MHWs as any day when local SST exceeds the seasonally varying 99th percentile within an 11 day moving window relative to the 1991-2020 climatology. Monthly cumulative MHW intensity is defined as the sum of the SST anomalies for each MHW day. This combines both the number of days spent in a MHW state and the intensity of those days above the climatological mean, providing an indicator of accumulated heat stress (Jacobs et al., 2024).

MHW activity becomes noticeably greater later in the record in all regions (figure 2.6). Before the 2000s, monthly cumulative intensities above 20°C·days were rare in all four regions, whereas values over 40°C·days now occur repeatedly in recent summers. The western Mediterranean stands out most clearly, with relatively frequent MHW conditions and stronger SST anomalies. In recent years, June and July cumulative intensities often reached over 60°C·days, alongside average SST anomalies of 2-3°C or more. July 2026 stands out across several regions, recording the highest July cumulative intensity for the Celtic region, at 40°C·days, the Bay of Biscay & Iberian Peninsula, at 60°C·days, and the western Mediterranean at 90°C·days.

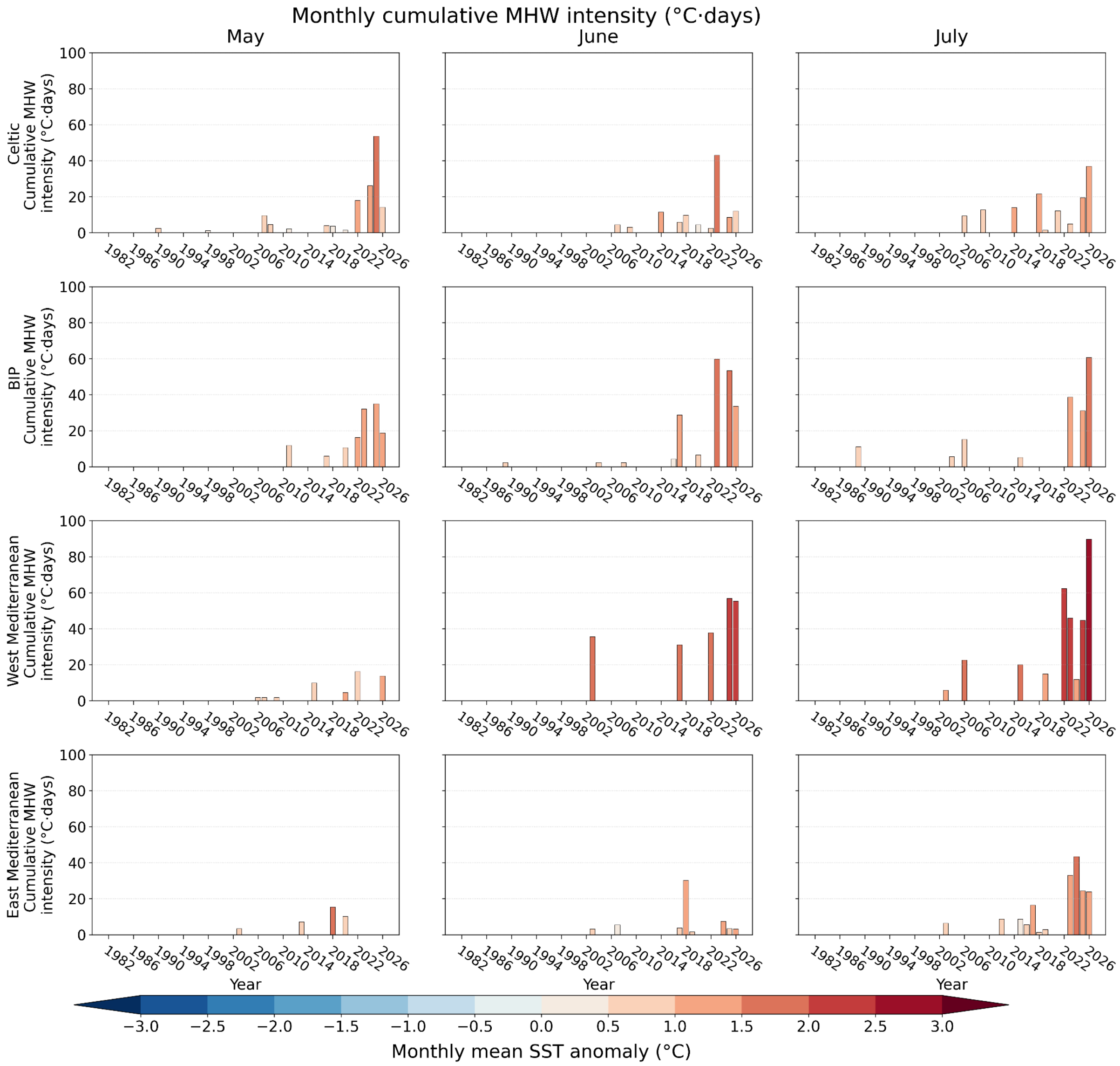

Figure 2.6: *Monthly cumulative MHW intensity for May, June, and July in the four study regions (cumulative MHW intensity calculated as sum of the SST anomaly of each MHW day), calculated using NOAA OISSTv2 SST dataset. Bar colours indicate the corresponding monthly mean SST anomaly relative to the 1991-2020 climatology.*

2.4 Summary of observed changes

Despite the extreme nature of the 14-day annual SST maximum events across the four regions, the values observed in July 2026 (some weeks prior to the typical annual maxima being reached) are relatively common in today's climate, with return periods of 1.5 to 5 years. For both the Celtic and BIP regions the observed changes in intensity are approximately in line with global warming, approximately 1.4°C. In contrast, observed intensity changes for both Mediterranean regions are far above global warming, with temperature increases ranging between 2.9°C and 3.4°C for the eastern and western regions respectively.

While relatively common events today, the SST14x was far less common in a 1.4°C cooler climate. In the Celtic region, the lowest rate of change was found. This is likely due to the pronounced decadal-scale variability, linked to Atlantic Multidecadal Variability. Temperature changes are at an approximately average warming rate of 1.5°C and the probability ratio is roughly 30, suggesting this would have been a roughly 1-in-100 year event in a pre-industrial climate - rare but not impossible, experienced maybe once in a typical human lifetime. In contrast, the SST14x experienced in the three other regions were virtually impossible in a preindustrial climate. Observations suggest temperatures in the BIP region have increased by 1.7°C, in WMed by 3.4°C and in EMed by 2.9°C.

Focusing on SST14x for the July month exclusively (SST14x-July), which enables a more like-for-like comparison given that annual SSTs typically peak only in late summer, we see that 14-day maximum SSTs are much rarer when occurring this early in the season. There is also a stronger variance of absolute likelihood by basin, with the most extreme variance in the present climate in the BIP region. One outlier is found in the eastern Mediterranean region where SST14x for July as experienced this year is still a relatively common event. July has the fastest rate of change in SST14x for all four regions. The Celtic region also has less decadal variability when compared to the yearly SST14x event definition. Across all four regions, the observations suggest that these July events would have been virtually impossible in a preindustrial climate.

Next, observations were used to ascertain changes in SSTs per calendar month. We found that increases in shoulder month (May - June and September - November) temperatures are evident in all four regions. Most surprising is an increase for both sets of shoulder months for the BIP region greater than for summer temperatures, while the other three regions saw increases for the early summer months. While all months are seeing an increase in SSTs, summer is generally warming much faster than winter. This is particularly true for both Mediterranean regions.

Finally, a brief overview of MHWs was carried out for the four regions. Before the 2000s, cumulative intensities above 20°C·days were rare. Over recent years we see hotter and more sustained MHWs for both June and July, with July 2026 recording the highest July cumulative intensity for the Celtic, BIP and western Mediterranean regions respectively and the third highest for the eastern Mediterranean.

3 Attribution of trends

3.1 Multi-model attribution using WWA protocol

All climate models used are outlined in detail in Appendix A1.2.

3.1.1 Evaluation of climate models

In the subsections below we show the results of the model evaluation for each location. The climate models are evaluated against the observations in their ability to capture:

1. Seasonal cycles: For this, we qualitatively compare the seasonal cycles based on model outputs against observations-based cycles. We discard the models that exhibit ill-defined peaks or troughs in their seasonal cycles with respect to the observations.

2. Spatial patterns: Models that do not match the observations in terms of the large-scale SST patterns are excluded.

3. Parameters of the fitted statistical models. We discard the model if the model and observation parameters ranges do not overlap.

The models are labelled as 'good', 'reasonable', or 'bad' based on their performances in terms of the three criteria discussed above. A model is given an overall rating of 'good' if it is rated 'good' for all three characteristics. If there is at least one 'reasonable', then its overall rating will be 'reasonable' and 'bad' if there is at least one 'bad'. For each framing or model setup we also use models that only just pass the evaluation tests if we only have five models or less for that framing that perform well. Overall, 5 of the 12 models were retained for the Celtic, BIP and WMed regions and 9 of the 12 were restrained for the EMed region in this study. Tables of the model evaluation results can be found in Appendix A3.

3.1.2 Synthesis of results

For the event definitions described and analysed in Section 2 we evaluate the influence of anthropogenic climate change on the events by calculating the probability ratio as well as the change in intensity using both observations and climate models. Models which do not pass the evaluation described above are excluded from the analysis. The aim is to synthesise results from models that pass the evaluation along with the observations-based products, to give an overarching attribution statement. Tables of the results of this model fitting can be found in Appendix A4.

Figures 3.1-3.4 show the changes in probability and intensity for the observations (blue) and models (red). Before combining them into a synthesised assessment, first, a representation error is added (in quadrature) to the observations, to account for the difference between observations-based datasets that cannot be explained by natural variability. The dark blue bar shows the average over the observation-based products, including this additional variability. Next, a term to account for intermodel spread is added (in quadrature) to the natural variability of the models. The dark red bar shows the model average, consisting of a weighted mean using the (uncorrelated) uncertainties including this natural variability, plus the term representing intermodel spread. Observation-based products and models are combined into a single result by computing the weighted average of models (dark red bar) and observations (dark blue bar): this is indicated by the magenta bar.

Results for the Celtic and BIP regions can be found in Table 3.1. While changes in the Celtic region are less pronounced than the other three regions, in a world without human-caused global warming similarly extreme 14-day annual-high SST values would only have been expected once in approximately 100 years. Currently, these temperatures are expected once every 3 years, and with continued warming to 2.8°C we expect similarly extreme SST events to occur almost every year. The synthesised SSTs, from a preindustrial climate to present, are increasing approximately in line with global warming. The Bay of Biscay and Iberian Peninsula region region has also seen stark change in the likelihood of similarly extreme 14-day annual-high SSTs since pre-industrial times, reflected in a synthesised probability ratio of 240; we note that the observed probability ratio is an order of magnitude higher than this, suggesting that the finding is probably conservative and underscoring the strength of the warming trend in this region. Without climate change, we would expect similar events to occur once in approximately 1,200 years, now these events occur once every 5 years.We would expect events at least this hot to occur almost every year with a further 1.4°C of warming from today in both regions.

Data	**Period**	**Celtic**		**Bay of Biscay & Iberian Peninsula**	
		Probability ratio (95% CI)	**Intensity change (°C) (95% CI)**	**Probability ratio (95% CI)**	**Intensity change (°C) (95% CI)**
Observations	**Past - present**	**31.7 (2.59, 1180)**	**1.21 (0.30, 2.04)**	**2050 (10.7, >1m)**	**1.52 (0.77, 2.22)**
Models		47.7 (0.48, 6150)	**1.30 (0.42, 2.18)**	**101 (2.21, 5740)**	**1.27 (0.43, 2.09)**
Synthesis		**35.7 (1.37, 2000)**	**1.25 (0.36, 2.11)**	**240 (3.31, 39800)**	**1.41 (0.62, 2.16)**
Models only	**Present future**	**2.61 (2.24, 3.03)**	**1.15 (0.62, 1.68)**	**4.20 (3.62, 4.87)**	**1.17 (0.80, 1.53)**

***Table 3.1**: Summary of results for SST14x in the Celtic and BIP regions, including changes due to a 1.4°C increase in GMST from preindustrial to the present climate of 2026, combining observation-based and climate model datasets, and a further 1.4°C increase from present to a future climate, using climate model projections. Statistically significant changes at the 95% confidence level are highlighted in **bold text**.*

In the two Mediterranean regions climate models substantially differ with observations, by 3 to 4 orders of magnitude, in the probability ratio of the observed SST warming (Table 3.2).Both intensity change and probability ratios are reported similar to the first two regions, because models contribute more to the synthesised values than observations. For this reason, it must be noted that both Mediterranean region results possibly underrepresent the true changes being experienced in the respective regions. Both regions have warmed approximately 1.8°C in response to 1.4°C human-caused global warming and are expected to rise a further 1.7°C should we reach 2.8°C of warming globally. More concerning yet is the frequency at which these events are expected to occur. The west Mediterranean is currently experiencing more severe heat than the east. The 14-day SST observed in July 2026 in the west, which was expected to occur every 2000 years in a 1.4°C cooler climate, is currently a 1-in-5 year event. With further warming of 1.4°C we can expect similarly warm SSTs to become an almost annual event. In the east Mediterranean, the 14-day high SST's would have been expected to occur every 350 years without human-caused global warming, today it happens two out of every three years and in the future it will become an annual event. Once again, we see a much stronger trend in observations than in climate models, reflecting the strength of the warming trend and indicating that this should be interpreted as a conservative estimate of the change in likelihood.

Data	Period	Western Mediterranean		Eastern Mediterranean	
		Probability ratio (95% CI)	Intensity change (°C) (95% CI)	Probability ratio (95% CI)	Intensity change (°C) (95% CI)
Observations	**Past - present**	**183000 (32.7, >1m)**	**3.09 (1.68, 4.43)**	**81600 (2.67, >1m)**	**2.62 (1.12, 4.16)**
Models		**379 (107, 1810)**	**1.77 (1.36, 2.20)**	**188 (23.5, 2170)**	**1.70 (1.17, 2.22)**
Synthesis		**428 (75.0, 3910)**	**1.89 (1.31, 2.46)**	**237 (13.4, 7120)**	**1.79 (1.10, 2.50)**
Models only	**Present future**	**4.69 (4.48, 4.92)**	**1.73 (1.44, 2.03)**	**1.50 (1.50,1.50)**	**1.71 (1.22, 2.20)**

***Table 3.2**: Summary of results for SST14x in the Western and Eastern Mediterranean regions, including changes due to a 1.4°C increase in GMST from preindustrial to the present climate of 2026, combining observation-based and climate model datasets, and a further 1.4°C increase from present to a future climate, using climate model projections. Statistically significant changes at the 95% confidence level are highlighted in **bold text**. Probability ratios are reported for a 5-year and 1.5-year event in the WMed and EMed respectively, in the climate of 2026, meaning that future changes in likelihood are capped at 5 and 1.5 times more likely, respectively.*

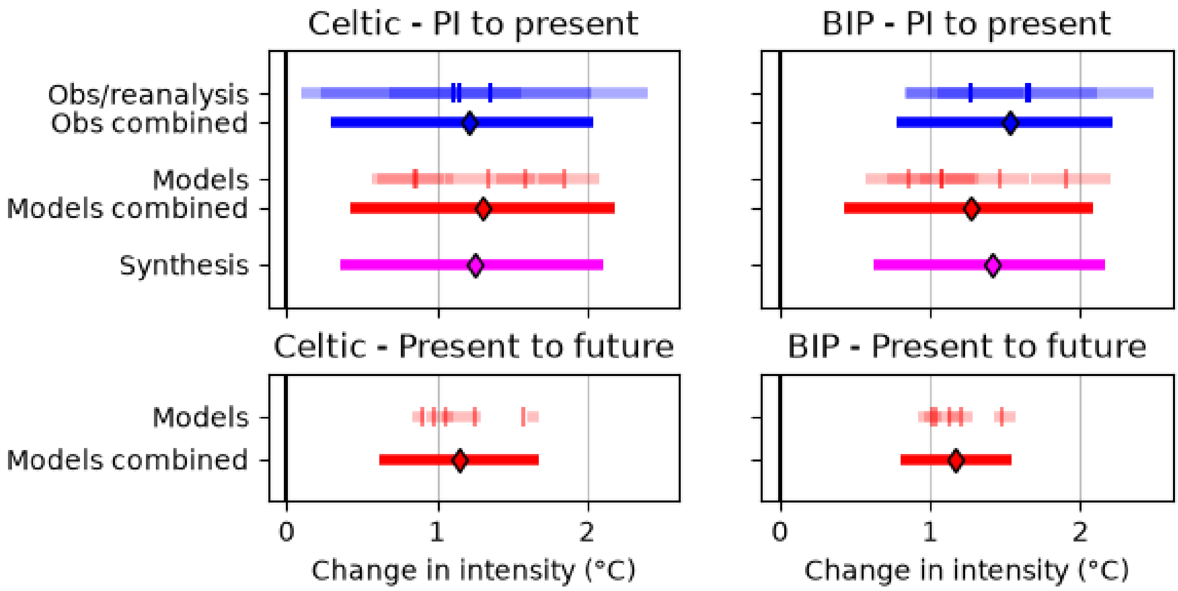

Figure 3.1: *Synthesis of change in SSTs in the Celtic and Biscay/Iberian Peninsula study regions. Shaded bars represent bootstrapped uncertainties in each dataset; vertical ticks indicate results for individual datasets; coloured diamonds represent synthesised results for each group. Top row: change in SSTs from preindustrial (1.4°C cooler than the present) to 2026; bottom row: projected change in SSTs from the present to a future 1.4°C warmer climate.*

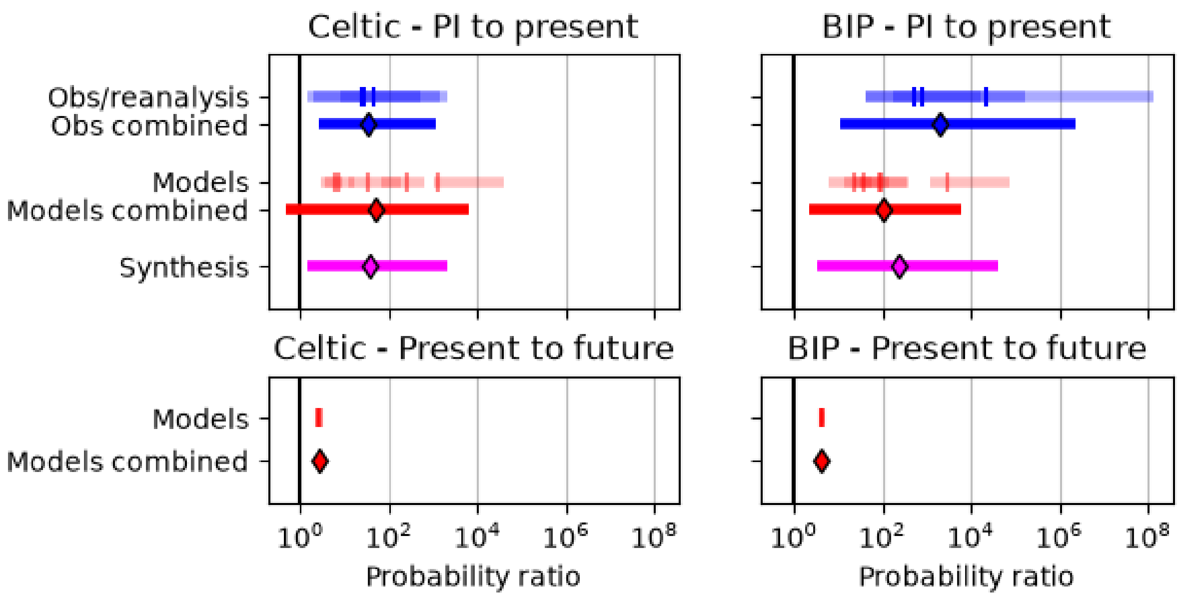

Figure 3.2: *Synthesis of change in likelihood of similarly extreme SSTs in the Celtic and Biscay/Iberian Peninsula study regions. Shaded bars represent bootstrapped uncertainties in each dataset; vertical ticks indicate results for individual datasets; coloured diamonds represent synthesised results for each group. Top row: change in likelihood from preindustrial (1.4°C cooler than the present) to 2026; bottom row: projected change in likelihood from the present to a future 1.4°C warmer climate.*

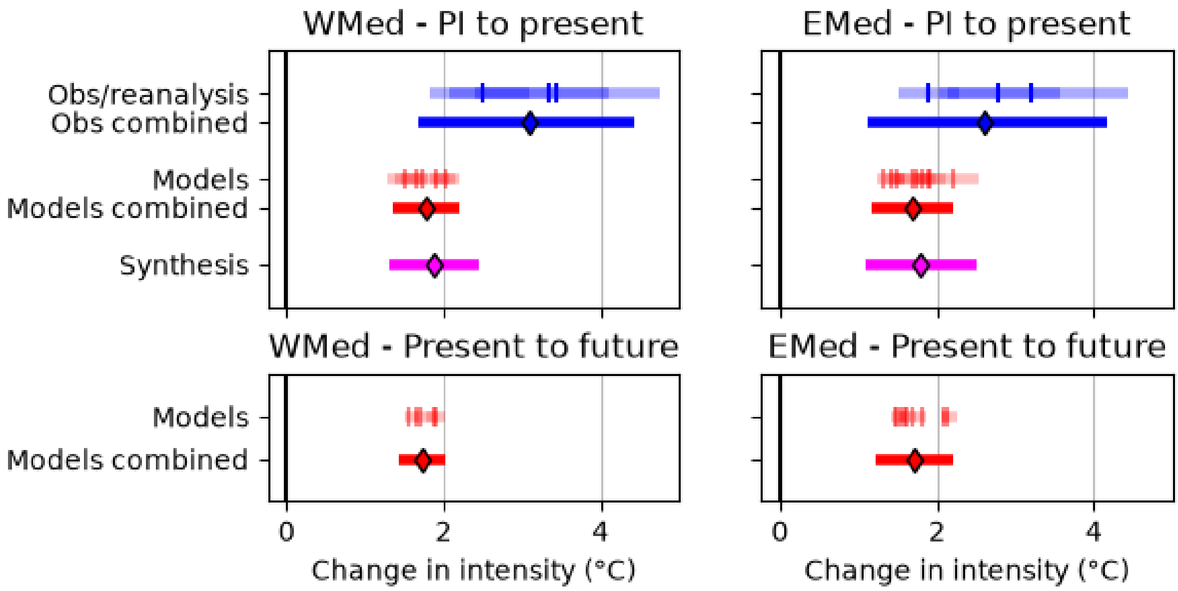

Figure 3.3: *As Figure 3.1, but for the two Mediterranean study regions.*

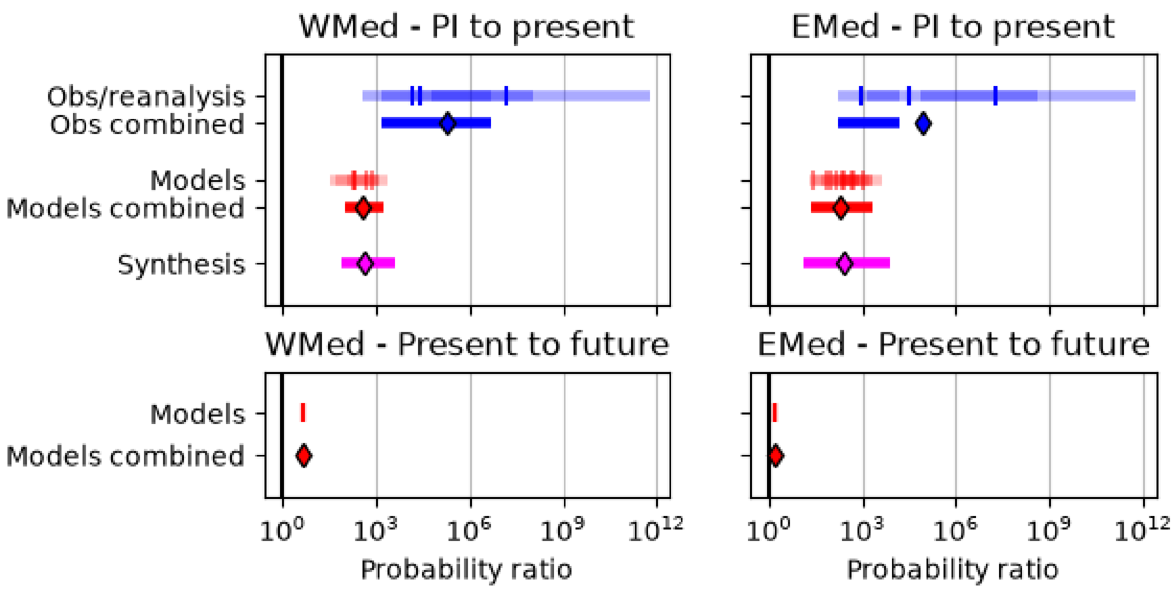

Figure 3.4: *As Figure 3.2, but for the two Mediterranean study regions.*

3.2 Complementary attribution using Climate Central's Climate Shift Index system

Climate Central's Climate Shift Index (CSI) system quantifies the contribution of climate change to daily observed SSTs in near-real time. The foundations for this system were first published by Giguere et al. (2024). The CSI methodology is complementary to the WWA protocol, enabling a comparison between methods. In addition to reporting attribution information for each of the study regions, we also use the CSI system to quantify the contribution of climate change to MHW conditions in each region. For the purposes of this analysis, we adopt the MHW definition established by Hobday et al. (2016). To meet the criteria for a MHW, sea surface temperatures must exceed the local 90th percentile threshold from the fixed 1982-2011 climatology for at least five days. Events separated by gaps of two days or fewer below the threshold are treated as part of the same continuous event.

Ocean CSI data indicate that climate change increased both the likelihood and the intensity of the observed warm temperatures in each region (Table 3.3). Ocean CSI values for the 14-day period analyzed for each region ranged from 22 in the Celtic region to 155 in the Eastern Mediterranean—indicating that climate change made the observed SSTs in those regions 22 times more likely and 154 times more likely, respectively (Figure 3.5). Across all four regions, observed SST anomalies averaged 2.4°C, with 1.6°C of that anomaly attributable to climate change. In other words, climate-change-driven warming accounted for about two-thirds of the observed anomaly overall, with the remainder of the anomaly resulting from natural climate variability and/or short-term weather and oceanographic conditions. The contribution of climate change ranged from 1.1°C of the 1.9°C anomaly in the Celtic region to the entirety of the 2.0°C anomaly in the Eastern Mediterranean.

Our MHW analysis shows that climate change increased the extent of MHWs in each region, see Figure 3.6. For example, nearly 90% of the Bay of Biscay and Iberian Peninsula region met the criteria for a MHW during the 14-day study period. In a counterfactual climate without human-caused climate change, less than 40% of the area would have been experiencing such conditions. The MHW in the Eastern Mediterranean demonstrates a high degree of attributability to climate change. While 65% of the region experienced MHW conditions during the 14-day study period, only 9% of the region would have experienced such conditions in the absence of climate change.

Region	**Mean Ocean CSI Value**	**Change in SST intensity due to climate change (°C)**	**Observed: Percent of area experiencing MHW conditions (%)**	**Counterfactual: Percent of area that would have experienced MHW conditions (%)**
Celtic	21.8 (19.8, 23.8)	1.1	79.8 (73.1, 86.4)	26.3 (22.8, 30.5)
Bay of Biscay & Iberian Peninsula	32.1 (26.1, 38.1)	1.1	89.3 (88.2, 90.5)	38.2 (32.3, 44.0)
Western Mediterranean	91.1 (80.2, 102)	2.0	79.4 (78.8, 80.0)	41.3 (35.0, 47.6)
Eastern Mediterranean	154 (118, 189)	2.0	67.2 (62.8, 71.3)	8.4 (5.3, 11.6)

Table 3.3: *Summary statistics from Climate Central's Climate Shift Index system. Values represent averages across each region and 14-day analysis period. Ranges in parentheses show the 95% confidence interval around the 14-day mean, calculated from day-to-day variability during the period.*

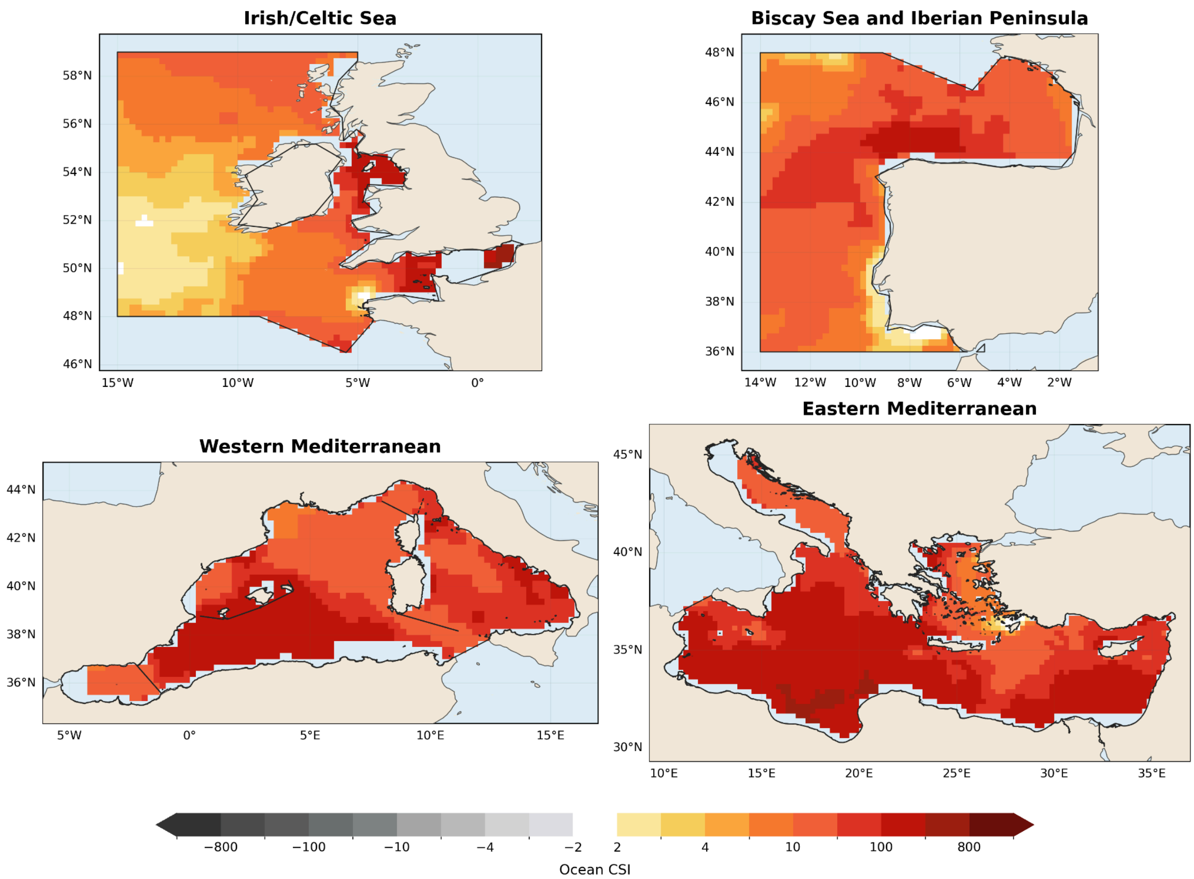

Figure 3.5: *Mean ocean CSI values from Climate Central's Climate Shift Index system for each of the four study regions and 14-day time periods. Ocean CSI values represent the number of times more (or less) likely observed SSTs were as a result of climate change.*

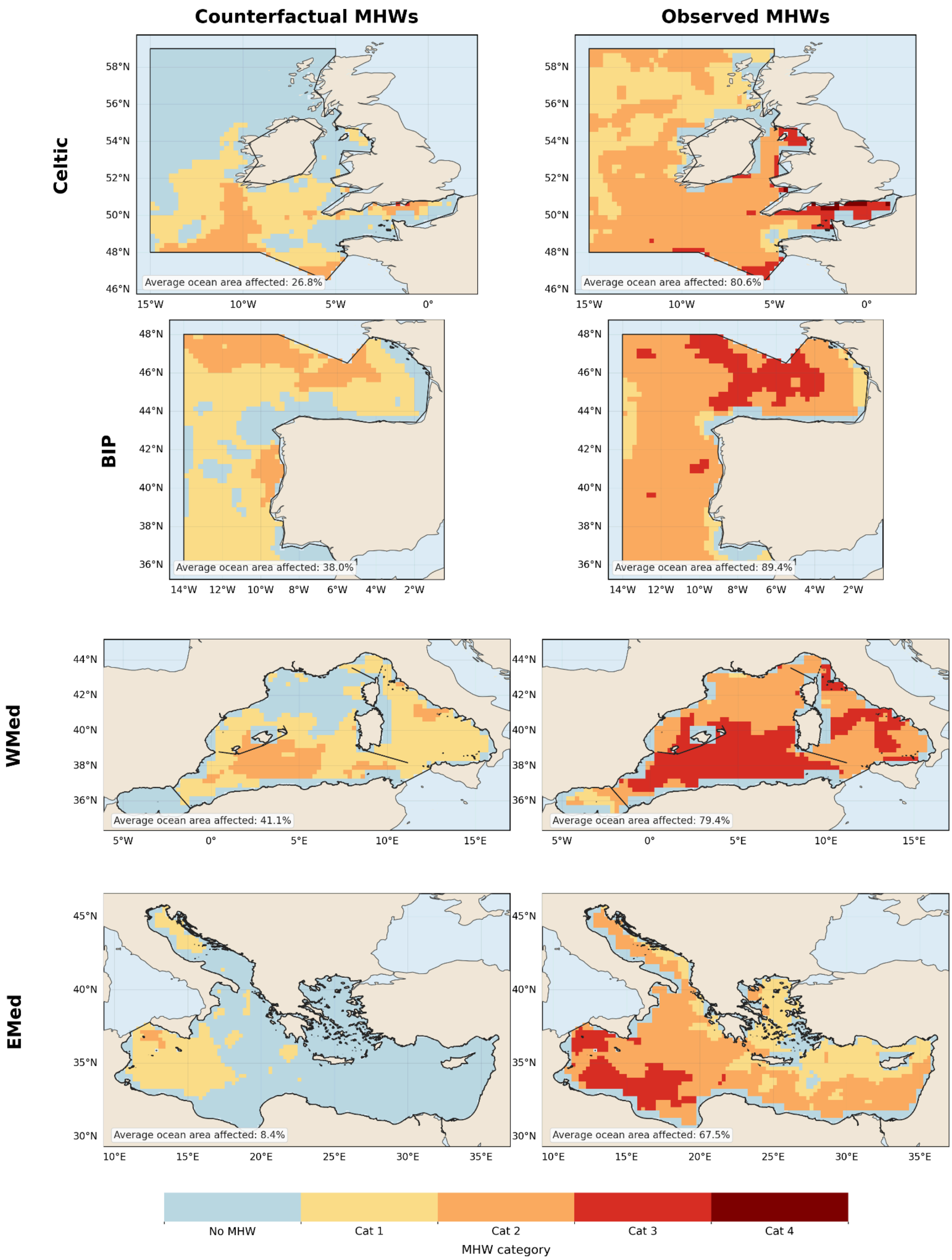

Figure 3.6: *Average observed marine heatwave category and counterfactual marine heatwave category for each of the four study regions and 14-day periods. Marine heatwave categories are based on observed SSTs relative to a fixed 1982-2011 climatology, and we consider a MHW attributable to climate change when observed SSTs were made at least six times more likely by climate change according to Ocean CSI. Values represent the average daily MHW category across the analysis period.*

3.3 Conclusions hazard

While the 14-day annual maximum SST values across all four regions around Europe are now common events, with return periods between 1.5 and 5 years, they were much rarer in a pre-industrial climate. For the Celtic region, a now 1-in-3 year event was expected approximately once a century in a preindustrial climate. In comparison, the 14-day max SSTs now experienced in the eastern Mediterranean are almost yearly events, despite them being very uncommon, once every 350 years, in the past. Of most concern are the changes seen for the western Mediterranean and Bay of Biscay and Iberian Peninsula regions. While both regions have very common high temperatures today, in a 1.4°C cooler climate these same 14-day maximums would be extremely unlikely, happening once every 1,000 to 2,000 years. With further warming, 2.8°C above the preindustrial average , all four regions should expect these 14-day annual maximum SSTs to happen almost every year. Climate Central's CSI data also indicates that the observed 14-day SST values during July are increasingly likely because of climate change. Across all four regions, climate change made the observed SSTs 22–155 times more likely under this alternative metric. Irrespective of choice of method the message is stark: high SSTs, such as those seen in July 2026 around Europe have become a common occurrence.

In addition to the likelihood of these events changing with human-caused climate change, we also detect an increase in the event's extreme temperatures of 1-2°C. Both the Celtic and Bay of Biscay and Iberian Peninsula regions are warming roughly in line with global warming, this should continue to occur as our world continues to warm. Both regions in the Mediterranean are heating at a greater rate than global warming, despite ocean temperatures increasing on average more slowly than land, this trend is expected to continue with future warming. Further analysis showed that the extent of MHWs increased across all regions. The smallest changes were seen in the western Mediterranean where 41% MHW coverage would have been expected in a pre-industrial time is now 79% and the largest change was in the eastern Mediterranean which went from 8% to 67%.

4 Vulnerability and exposure

Marine heatwaves (MHWs) are prolonged periods of unusually warm seawater, typically defined as temperatures exceeding the expected seasonal range (hotter than 90% of days) for at least five consecutive days (Hobday et al., 2016; KNMI, 2026). As oceans retain heat longer than air, MHWs can persist for weeks to months, with warming coastal waters particularly exposed (KNMI, 2026).

Beyond physiological stress and mortality, extreme warming can reorganize marine communities, shift the distribution of species, and disrupt fisheries and aquaculture, with consequences extending well beyond the marine environment (Bonino et al., 2025). The Mediterranean has experienced several notable events, including 1999, 2003, 2007, 2020, and 2022 (Garrabou et al., 2022; Bonino et al., 2025), with the 1999 and 2003 events affecting more than 40 species (Garrabou et al., 2022).

This chapter examines vulnerability and exposure to Mediterranean MHWs across wildlife, livelihoods, food systems, and human health, including cascading impacts and risks connecting these systems.

4.1 Wildlife, livelihoods, and food system

Marine heatwaves can rapidly alter Mediterranean ecosystems, and does so with an accelerating pace (Garrabou et al., 2022). Impacts range from mass mortality of fish, invertebrates, seabirds, and marine mammals, to coral bleaching and declines in seaweeds and seagrasses (Capotondi et al., 2024; Wilson et al., 2025). Benthic species that live on or near the seafloor, such as corals and shellfish, are particularly vulnerable because they cannot move easily to cooler waters. Species that grow slowly may also take longer to recover after being exposed to extreme temperatures (Wilson et al., 2025). These ecological changes can also shift species distributions and favor invasive species, altering marine communities and the availability of commercially important species (Fraser, 2026). For example, invasive pufferfish are predators that can compete with or prey on native and valuable fish, adding pressure to already-stressed fisheries (Stellacci & Hadjicostis, 2026; Dunphy, 2026). Warming can thus create favorable conditions for some species, with events such as the reported "octopus bloom" demonstrating how MHWs can temporarily increase the abundance of particular species (UK Gov, 2026).

These changes have direct implications on livelihoods and food systems. Shifts in fish abundance and distribution can reduce catches, increase fishing effort and costs, and undermine the incomes and food security of coastal communities. MHW-induced ecosystem changes may also interact with other pressures, including invasive species. The Asian brown alga *Rugulopteryx okamurae*, first detected in the Strait of Gibraltar in 2015, has since spread extensively across the Mediterranean and Atlantic coasts (Souviron-Priego et al., 2024; Laamraoui et al., 2024). Large quantities also accumulate on beaches, creating significant removal costs and affecting tourism and fishing activities (Ibid.). Recent evidence of its continued northward expansion along the Spanish Mediterranean coast highlights the ongoing nature of this pressure (Burgen, 2026).

4.2 Human health

Despite increases in the intensity, frequency, and duration of marine heatwaves, the linkages between human health consequences still remain under-studied (Falkenberg & Russell, 2026). Marine heatwaves can directly impact the physical and mental health of populations via effects to the physical environment, including amplification of extreme weather events, such as atmospheric heatwaves and storms, resulting in increases in morbidity and mortality (Falkenberg & Russell, 2026). The concurrence of marine and atmospheric heatwaves has also been identified as an emerging public health risk (Pastor et al. 2024; Falkenberg & Russell, 2026). Warming seas can aggravate tropical nights, compounding extreme heat events and reducing people's ability to recover at night (Dailidienė et al. 2025; UK Met Office, 2025; Il Mattino, 2026).

Indirect impacts can also occur due to disruptions to ecosystem services, such as increases in harmful algae blooms (HABs) and spread of pathogens impacting water quality and food resources, often with implications to social and economic systems (Falkenberg & Russell, 2026). Increasing sea surface temperatures help *Vibrio* bacteria multiply rapidly leading to severe gastrointestinal illnesses and skin infections for people who swim in or handle contaminated water, as well as through consumption of contaminated raw or undercooked seafood (particularly shellfish) (Schets et al. 2025). In Europe, increases in non-cholera Vibrio have been observed related to exposure to surface water and ocean warming (Baker-Austin et al. 2012; Thykjaer, 2026). HABs, linked to marine heatwaves also produce potent toxins that accumulate in fish and shellfish and when ingested, these toxins can lead to significant and severe health consequences, including neurological impairment and death (Landrigan et al. 2020). Additionally, HABs disrupt aquaculture and fishing industries, impacting local livelihoods and access to vital marine protein sources, as well as threatening global nutrition and food security (Falkenberg & Russell, 2026, University of Adelaide, 2026). Impacts on mental health and well-being related to loss of marine ecosystems for communities whose livelihoods and cultural identity are closely linked to the ocean have also been highlighted (Falkenberg & Russell, 2026; Le Busque et al. 2026).

4.3 Cascading impacts

The cascading impacts of marine heatwaves are increasing and affecting different sectors. In relation to biodiversity, it is linked to mass mortality events (e.g. *Posidonia oceanica* decrease), shifts in species distributions and seasonal timing, and disruption to ecosystem functioning, including food web dynamics, productivity and biogeochemical cycles (Copernicus, 2025). In addition, it has significant impact on tourism, fisheries and coastal communities' economy and livelihoods across the Mediterranean Sea (Schroeder et al., 2024).

For instance, the increasing marine heatwaves in the eastern and northern coasts of Sicily and the northern Adriatic coast are producing the increase of *H. carunculata and C. sapidus* (respectively). The proliferation of *C. sapidus* significantly disrupted mussel production, benthic habitats, altering community composition and leading to remarkable changes at the level of the entire food web (Martelucci et al., 2025). In the case of *H. carunculate*, it poses a threat to both marine biodiversity and the economic stability of local fisheries. The fireworm directly damages the severing of secondary lines attached to hooks, either by the worm's teeth or by hiding among the rocks after consuming the bait. In response, the soaking time of the fishing gear has been reduced, which leads to a decrease in catch rates, affecting the efficiency of fisheries, and impacting the fishing industry by damaging fish catches and reducing the market value of fish (Martelucci et al., 2025). The economic impact is estimated at around EUR 7.32 kg^{-1} of damaged fish, resulting in significant annual losses given the total weight of commercially valuable catches (Tiralongo et al., 2023).

In relation to tourism, the increase of marine heatwaves, combined with factors like loss of biodiversity, reduction in cleanliness and acidification are impacting tourism trends and value of sea activities and sports in Europe (González Hernández et al., 2022).

Finally, in places like Hungary, due to the record-low water levels of the Danube, limited cooling water available and high the temperature of the Danube, a nuclear power plant had to largely shut down operations (DW, 2026)

4.4 Adaptation to marine heatwaves

While some species may be able to adapt or acclimate to warmer temperatures, the increasing length, frequency and intensity of these events are pushing some marine ecosystems beyond what they can tolerate (Cooley et al., 2022). Adaptation solutions can include reducing additional pressures on marine ecosystems, protecting climate refugia, adapting fisheries and aquaculture management, and improving monitoring and early-warning systems (Cooley et al., 2022).

5 Conclusions

Overall, the analyses undertaken demonstrates that very high SSTs and marine heatwave conditions are becoming increasingly common in all analysed regions, and a defining feature of the Mediterranean's changing climate rather than isolated extreme events. Their increasing frequency, intensity, duration and spatial extent are already reshaping marine ecosystems and creating cascading risks for fisheries, food security, tourism, coastal livelihoods and human health. These impacts are interconnected: ecological disruption can undermine livelihoods and food systems, while warming seas can simultaneously increase direct and indirect risks to human health. Adaptation measures - mainly reducing additional anthropogenic pressures, protecting climate refugia, strengthening fisheries and aquaculture management, and improving monitoring and early-warning systems - will be essential to reduce vulnerability and build resilience. However, the rapidly increasing likelihood of extreme marine temperatures highlights the limits of adaptation alone. Without a rapid transition away from fossil fuels, marine heatwaves will continue to intensify and become increasingly commonplace, progressively narrowing the capacity of Atlantic and Mediterranean ecosystems and the societies that depend on them to cope.

Data availability

All time series used in the attribution analysis are available via the Climate Explorer.

Acknowledgements

Claire Bergin acknowledges the WASITUS project funded by the EPA and Met Éireann (Grant number: 2024-CE 1265).

This work used JASMIN, the UK's collaborative data analysis environment (https://www.jasmin.ac.uk).

This work used resources of the Deutsches Klimarechenzentrum (DKRZ), granted by its Scientific Steering Committee (WLA) under project ID bk1088 and datasets provided by ESGF/Copernicus via the DKRZ data pool.

This work used Imperial College Research Computing Service, DOI: 10.14469/hpc/2232.

This work used the KNMI Climate explorer web tool (https://climexp.knmi.nl/start.cgi).

References

All references are given as hyperlinks in the text.

Appendices

A1 Data and methods

A1.1 Observational data

We first use observational and reanalysis data to estimate the return period of a similar event in the present day and to assess the historical trends with increasing GMST. The datasets used are as follows:

- **ERA5** - The European Centre for Medium-Range Weather Forecasts's 5th generation reanalysis product, ERA5, is a gridded dataset that combines historical observations into global estimates using advanced modelling and data assimilation systems (Hersbach et al., 2020). We use sea surface temperature data from this product at a resolution of 0.25°×0.25° from the years 1940 to July 2026.
- **OISST** - The NOAA Optimum Interpolation Sea Surface Temperature, OISST v2, is a high-resolution (0.25°×0.25°) blended analysis of daily SSTs and sea ice based on data from multi-satellite sensors, ships, buoys and Argo floats (Huang et al., 2021).
- **OSTIA** - The Operational SST and Ice Analysis is a satellite and in-situ foundation SST analysis created using re-processed ESA SST CCI, C3S, EUMETSAT and REMSS satellite data and in situ data from the HadIOD dataset. The product is available from 1st October 1981 on a global regular grid at 0.05° resolution, and we use data regridded to 0.25°×0.25° (Worsfold et al., 2024).
- **HadISST** - The UK Met Office's gridded SST product, combining measurements from ships, drifting and moored buoys and satellite data. Gridded data are reconstructed using a two stage reduced-space optimal interpolation procedure, followed by superposition of quality-improved gridded observations onto the reconstructions to restore local detail (Rayner et al., 2003).
- **ERSST** - NOAA's Extended Reconstructed Sea Surface Temperature (ERSST), combining data from multiple sources into a reanalysis of SSTs from 1850 to the present at 2°×2° spatial resolution (Huang et al., 2025a and 2025b).

As a measure of anthropogenic climate change we use the global mean surface temperature (GMST), where GMST is taken from the National Aeronautics and Space Administration (NASA) Goddard Institute for Space Science (GISS) surface temperature analysis (GISTEMP, Hansen et al., 2010 and Lenssen et al. 2019). To remove the effect of the El Niño - Southern Oscillation on global mean temperatures, we use a four-year running mean of the annual GMST, centred on the third year.

A1.2 Model and experiment descriptions

We use simulated SSTs from twelve climate model realisations from the CMIP6 climate modelling experiment (Eyring et al., 2016). For all simulations, the period 1850 to 2014 is based on historical simulations, while the SSP5-8.5 scenario is used for the remainder of the 21st century.

A1.3 Statistical methods

Methods for observational and model analysis and for model evaluation and synthesis are used according to the World Weather Attribution Protocol, described in Philip et al., (2020), with supporting details found in van Oldenborgh et al., (2021), Ciavarella et al., (2021), Otto et al., (2024) and here. The key steps, presented in sections 3-6, are: (3) trend estimation from observations; (4) model validation; (5) multi-model attribution; and (6) synthesis of the attribution statement.

In this report we analyse time series of annual and July-only 14-day maximum sea surface temperatures averaged over the four study regions: Celtic, Bay of Biscay & Iberian Peninsula, Eastern and Western Mediterranean; SST14x and SST14X-Jul. For each time series we calculate the return period and intensity of the event under study for the 2026 GMST and for 1.4°C cooler GMST: this allows us to compare the climate of now and of the preindustrial past without human-caused warming (based on Forster et al., 2026), by calculating the probability ratio (PR; the factor-change in the event's probability) and change in intensity of the event.

A nonstationary normal distribution is used to model these time series. The distribution is assumed to shift linearly with the covariates, while the variance remains constant. The variable of interest, SST14x, is assumed to follow a normal distribution in which the location parameter varies with GMST:

$$X \sim N(\mu, \sigma \mid \mu_0, \sigma_0, \alpha, T),$$

where X denotes the variable of interest, sea surface temperatures; T is the smoothed GMST; μ_0 and σ_0 are the location and scale parameters of the nonstationary distribution; and α is the trend due to GMST. As a result, the location of the distribution has a different value in each year, determined by the GMST state. Maximum likelihood estimation is used to estimate the model parameters, with

$$\mu = \mu_0 + \alpha T \qquad \text{and} \qquad \sigma = \sigma_0.$$

A1.4 Ocean CSI

Climate Central's Climate Shift Index: Ocean (Ocean CSI) tool is used to rapidly compute the influence of human-caused climate change on Sea Surface Temperatures in the study regions. The methodology underpinning this attribution tool is based on peer-reviewed research (Giguere et. al, 2024). It uses a combination of an empirically-driven attribution method using OISST data (Huang et. al, 2021), and model simulations using an ensemble of 12 debiased CMIP6 models. Results from these two methods are aggregated to compute a single metric measuring the increase in likelihood of an SST occurring as a result of climate change.

This metric, called the Ocean CSI, is the ratio of the probability of a temperature occurring in today's climate to the probability of that same temperature occurring in a world without human-caused climate change. In addition to likelihood changes, the methods used to compute the Ocean CSI can be used to measure the temperature increase in a location on a given day due to climate change (Giguere et. al, 2024). This allows us to calculate the specific difference between an observed daily temperature in a location and what that temperature would have been in a counterfactual world without climate change. We estimate both the Ocean CSI and this climate-driven warming in the study regions. The Ocean CSI uses 0.25° by 0.25° latitude-longitude grid cells. For each point along the track, we found the cell and corresponding daily metrics closest to the centre of the storm at that time.

A2 Additional figures

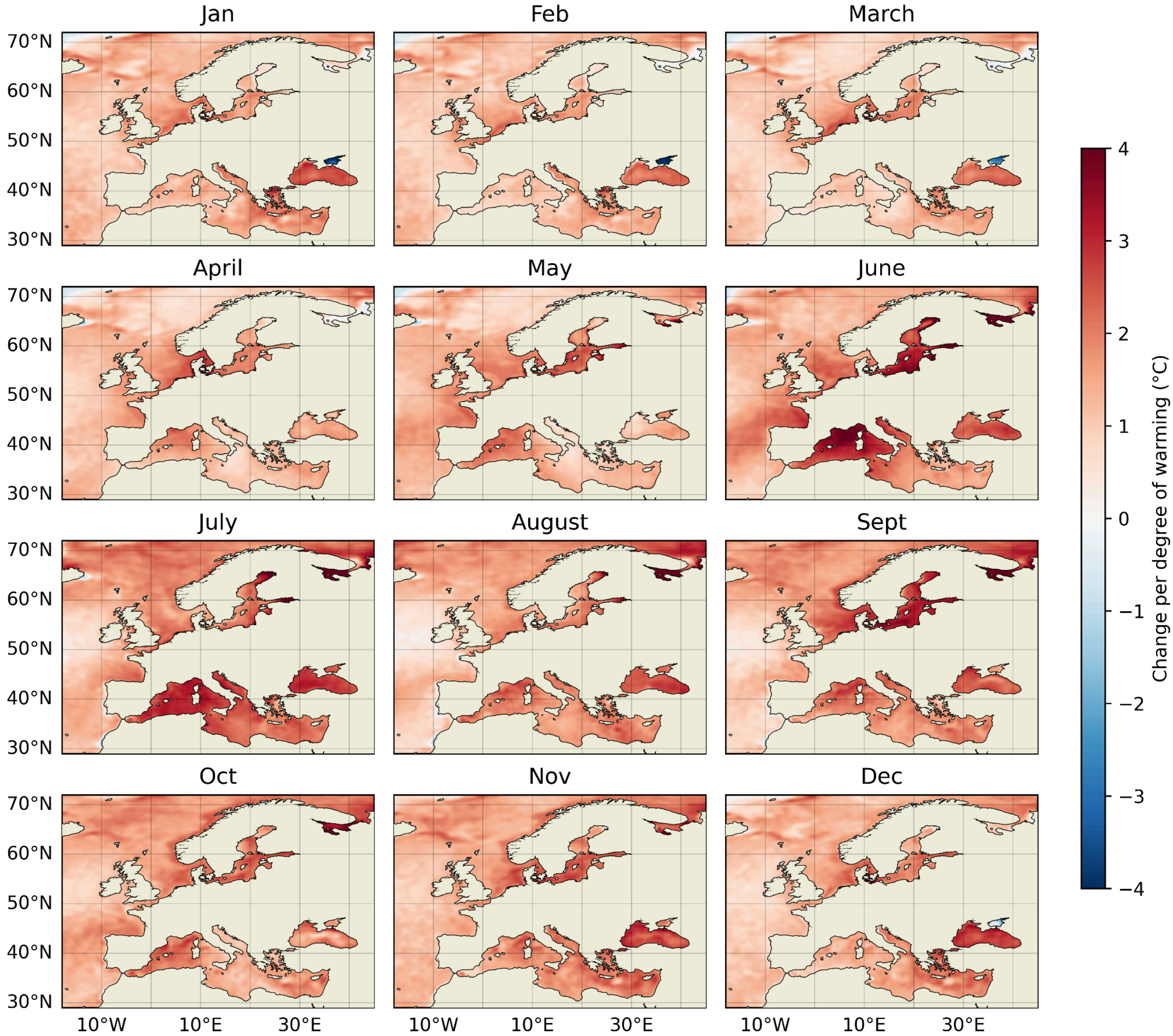

Figure A2.1: *Change in monthly mean temperature per degree of global warming at each gridpoint. Data: OISST.*

A3 Model evaluation tables

Model / Observations	Seasonal cycle	Spatial pattern	Dispersion	Conclusion
ERA5SST			0.59 (0.49…0.68)	
OISST			0.64 (0.5…0.72)	
OSTIA			0.71 (0.53…0.86)	
CanESM5_r10i1p1f1	bad	good	0.84 (0.77…0.87)	bad
CMCC-CM2-SR5_r1i1p1f1	good	good	0.79 (0.72…0.81)	good
CNRM-CM6-1_r2i1p1f2	bad	good	1.01 (0.9…0.98)	bad
CNRM-ESM2-1_r1i1p1f2	bad	good	0.84 (0.75…0.9)	bad
GFDL-CM4_r1i1p1f1	good	good	0.61 (0.51…0.69)	good
HadGEM3-GC31-LL_r1i1p1f3	good	good	0.67 (0.64…0.7)	good
MIROC6_r1i1p1f1	bad	good	0.72 (0.63…0.73)	bad
MPI-ESM1-2-LR_r10i1p1f1	good	good	0.6 (0.53…0.57)	good
MRI-ESM2-0_r1i1p1f1	good	good	0.55 (0.49…0.58)	good
NESM3_r1i1p1f1	bad	good	0.82 (0.76…0.83)	bad
NorESM2-LM_r1i1p1f1	bad	good	0.81 (0.74…0.84)	bad
NorESM2-MM_r1i1p1f1	bad	good	0.61 (0.55…0.64)	bad
UKESM1-0-LL_r1i1p1f2	good	good	0.9 (0.8…1)	reasonable

Table A3.1: *Evaluation results of the climate models considered for attribution analysis of SST14x Celtic. For each model, the threshold for a 1-in-3-year event is shown, along with the best estimates of the Dispersion parameters are shown, along with 95% confidence intervals. Furthermore evaluation of the seasonal cycle and spatial pattern are shown.*

Model / Observations	Seasonal cycle	Spatial pattern	Dispersion	Conclusion
ERA5SST			0.52 (0.44…0.58)	
OISST			0.48 (0.38…0.55)	
OSTIA			0.58 (0.42…0.72)	
CanESM5_r10i1p1f1	bad	good	0.74 (0.63…0.74)	bad
CMCC-CM2-SR5_r1i1p1f1	good	good	0.6 (0.52…0.62)	good
CNRM-CM6-1_r2i1p1f2	bad	good	0.84 (0.73…0.86)	bad
CNRM-ESM2-1_r1i1p1f2	bad	good	0.69 (0.61…0.73)	bad
GFDL-CM4_r1i1p1f1	good	good	0.63 (0.55…0.71)	good

HadGEM3-GC31-LL_r1i1p1f3	good	good	0.55 (0.47…0.58)	good
MIROC6_r1i1p1f1	good	good	0.53 (0.48…0.53)	good
MPI-ESM1-2-LR_r10i1p1f1	bad	good	0.77 (0.71…0.81)	bad
MRI-ESM2-0_r1i1p1f1	bad	good	0.47 (0.44…0.53)	bad
NESM3_r1i1p1f1	bad	good	1.08 (0.93…1.05)	bad
NorESM2-LM_r1i1p1f1	bad	good	0.89 (0.82…0.92)	bad
NorESM2-MM_r1i1p1f1	bad	good	0.61 (0.57…0.63)	bad
UKESM1-0-LL_r1i1p1f2	good	good	0.69 (0.62…0.76)	good

Table A3.2*: Evaluation results of the climate models considered for attribution analysis of SST14x BIP. For each model, the threshold for a 1-in-5-year event is shown, along with the best estimates of the Dispersion parameters are shown, along with 95% confidence intervals. Furthermore evaluation of the seasonal cycle and spatial pattern are shown.*

Model / Observations	**Seasonal cycle**	**Spatial pattern**	**Dispersion**	**Conclusion**
ERA5SST			0.74 (0.64…0.82)	
OISST			0.69 (0.54…0.82)	
OSTIA			0.91 (0.6…1.19)	
CanESM5_r10i1p1f1	good	good	0.59 (0.5…0.66)	good
CMCC-CM2-SR5_r1i1p1f1	good	good	0.69 (0.62…0.73)	good
CNRM-CM6-1_r2i1p1f2	bad	good	0.73 (0.63…0.82)	bad
CNRM-ESM2-1_r1i1p1f2	bad	good	0.51 (0.42…0.52)	bad
GFDL-CM4_r1i1p1f1	good	good	0.72 (0.71…0.77)	good
HadGEM3-GC31-LL_r1i1p1f3	good	good	0.72 (0.65…0.79)	good
MIROC6_r1i1p1f1	bad	good	0.88 (0.8…1)	bad
MPI-ESM1-2-LR_r10i1p1f1	good	good	0.8 (0.73…0.79)	good
MRI-ESM2-0_r1i1p1f1	bad	good	0.46 (0.42…0.45)	bad
NESM3_r1i1p1f1	reasonable	good	0.72 (0.6…0.74)	reasonable
NorESM2-LM_r1i1p1f1	bad	good	0.95 (0.95…1)	bad
NorESM2-MM_r1i1p1f1	bad	good	0.77 (0.7…0.81)	bad
UKESM1-0-LL_r1i1p1f2	bad	good	0.71 (0.66…0.77)	bad

Table A3.3*: Evaluation results of the climate models considered for attribution analysis of SST14x WMed. For each model, the threshold for a 1-in-5-year event is shown, along with the best estimates of the Dispersion parameters are shown, along with 95% confidence intervals. Furthermore evaluation of the seasonal cycle and spatial pattern are shown.*

Model / Observations	**Seasonal cycle**	**Spatial pattern**	**Dispersion**	**Conclusion**
ERA5SST			0.5 (0.42…0.57)	

OISST			0.44 (0.34…0.51)	
OSTIA			0.59 (0.39…0.76)	
CanESM5_r10i1p1f1	good	good	0.42 (0.37…0.44)	good
CMCC-CM2-SR5_r1i1p1f1	good	good	0.49 (0.45…0.53)	good
CNRM-CM6-1_r2i1p1f2	good	good	0.53 (0.51…0.58)	good
CNRM-ESM2-1_r1i1p1f2	good	good	0.41 (0.4…0.42)	good
GFDL-CM4_r1i1p1f1	good	good	0.53 (0.5…0.61)	good
HadGEM3-GC31-LL_r1i1p1f3	good	good	0.48 (0.42…0.51)	good
MIROC6_r1i1p1f1	bad	good	0.47 (0.44…0.51)	bad
MPI-ESM1-2-LR_r10i1p1f1	reasonable	good	0.43 (0.38…0.49)	reasonable
MRI-ESM2-0_r1i1p1f1	bad	good	0.37 (0.35…0.41)	bad
NESM3_r1i1p1f1	good	good	0.58 (0.55…0.67)	good
NorESM2-LM_r1i1p1f1	good	good	0.83 (0.76…0.89)	bad
NorESM2-MM_r1i1p1f1	good	good	0.54 (0.46…0.61)	good
UKESM1-0-LL_r1i1p1f2	good	good	0.56 (0.51…0.61)	good

***Table A3.4**: Evaluation results of the climate models considered for attribution analysis of SST14x EMed. For each model, the threshold for a 1-in-1.5-year event is shown, along with the best estimates of the Dispersion parameters are shown, along with 95% confidence intervals. Furthermore evaluation of the seasonal cycle and spatial pattern are shown.*

A4 Estimated trends in climate models

This section shows Probability Ratios and change in intensity ΔI for models that passed model evaluation and also includes the values calculated from the fits with observations.

		Preindustrial - Present (1.4˚C)		Present - Future (2.8˚C)	
Model / Observations	**Threshold for return period 3 yr**	**Probability ratio PR [-]**	**Change in intensity ΔI [˚C]**	**Probability ratio PR [-]**	**Change in intensity ΔI [˚C]**
ERA5SST	3.27˚C	44.57 (8.23…500.08)	1.15 (0.68…1.56)		
OISST	3.57˚C	28 (1.36…1999.67)	1.11 (0.1…2.03)		
OSTIA	2.47˚C	25.45 (1.93…1410.81)	1.36 (0.23…2.41)		
CMCC-CM2-SR5_r1i1p1f1	16.75˚C	5.62 (2.82…15.4)	0.85 (0.56…1.11)	2.51 (2.46…2.61)	1.06 (1.03…1.11)
GFDL-CM4_r1i1p1f1	16.83˚C	1250.67 (1030.41…39941.75)	1.85 (1.68…2.07)	2.93 (2.93…2.98)	1.57 (1.6…1.68)
HadGEM3-GC31-LL_r1i1p1f3	17.6˚C	31.95 (11.73…188.7)	1.34 (1.06…1.65)	2.68 (2.54…2.73)	1.25 (1.06…1.29)

MPI-ESM1-2-LR_r10i1p1f1	16.01˚C	7.07 (3.68…8.6)	0.86 (0.61…1.04)	2.45 (2.3…2.49)	0.91 (0.83…0.91)
MRI-ESM2-0_r1i1p1f1	17.58˚C	239.99 (67.81…637.78)	1.59 (1.39…1.83)	2.47 (2.42…2.59)	0.98 (0.93…1.05)

Table A4.1: *Event magnitude, probability ratio and change in intensity for 3-year return period for SST14x Celtic for observational datasets and each model that passed the evaluation tests. (a) from pre-industrial climate to the present and (b) from the present to 2.8℃ above pre-industrial climate.*

		Preindustrial - Present (1.4˚C)		**Present - Future (2.8˚C)**	
Model / Observations	**Threshold for return period 5 yr**	**Probability ratio PR [-]**	**Change in intensity ΔI [˚C]**	**Probability ratio PR [-]**	**Change in intensity ΔI [˚C]**
ERA5SST	6.18˚C	513.11 (42.2…15942.02)	1.27 (0.84…1.62)		
OISST	4.77˚C	21293.03 (174.15…136095824.74)	1.65 (1.04…2.11)		
OSTIA	3.38˚C	784.24 (41.49…163339.52)	1.64 (0.83…2.49)		
CMCC-CM2-SR5_r1i1p1f1	20.53˚C	22.73 (6.12…57.75)	0.85 (0.57…0.99)	4.14 (3.94…4.21)	1.01 (0.96…1.03)
GFDL-CM4_r1i1p1f1	22.46˚C	2891.58 (1216.67…74809.3)	1.91 (1.67…2.2)	4.63 (4.59…4.76)	1.47 (1.43…1.57)
HadGEM3-GC31-LL_r1i1p1f3	21.32˚C	36.87 (22.43…138.25)	1.07 (0.93…1.33)	3.89 (3.76…4.04)	1.04 (0.93…1.08)
MIROC6_r1i1p1f1	20.71˚C	81.63 (13.33…374.92)	1.08 (0.71…1.29)	4.44 (4.23…4.49)	1.13 (1.03…1.19)
UKESM1-0-LL_r1i1p1f2	21.63˚C	93.93 (29.5…349.93)	1.46 (1.1…1.66)	3.95 (3.89…4.11)	1.2 (1.12…1.28)

Table A4.2: *Event magnitude, probability ratio and change in intensity for 5-year return period for SST14x BIP for observational datasets and each model that passed the evaluation tests. (a) from pre-industrial climate to the present and (b) from the present to 2.8℃ above pre-industrial climate.*

		Preindustrial - Present (1.4˚C)		**Present - Future (2.8˚C)**	
Model / Observations	**Threshold for return period 5 yr**	**Probability ratio PR [-]**	**Change in intensity ΔI [˚C]**	**Probability ratio PR [-]**	**Change in intensity ΔI [˚C]**
ERA5SST	6.22˚C	24339.13 (1426.33…4675148.77)	2.5 (1.83…3.1)		
OISST	4.3˚C	16122850.82 (60846.93…669283400952.96)	3.33 (2.39…4.11)		

OSTIA	2.65˚C	15679.7 (352.04…103514276.35)	3.43 (2.07…4.76)		
CanESM5_r10i1p1f1	27.54˚C	194.37 (124.73…818.4)	1.51 (1.46…1.72)	4.78 (4.7…4.86)	1.65 (1.63…1.68)
CMCC-CM2-SR5_r1i1p1f1	28.74˚C	759.48 (447.13…1406.79)	2.02 (1.88…2.08)	4.77 (4.65…4.86)	1.89 (1.78…1.92)
GFDL-CM4_r1i1p1f1	27.26˚C	489.48 (838.02…2370.34)	1.9 (1.82…2.14)	4.66 (4.62…4.79)	1.71 (1.62…1.8)
HadGEM3-GC31-LL_r1i1p1f3	29.29˚C	210.22 (34.36…464.1)	1.66 (1.27…1.8)	4.52 (4.47…4.55)	1.54 (1.51…1.63)
MPI-ESM1-2-LR_r10i1p1f1	26.39˚C	181.7 (48.98…1122.23)	1.73 (1.37…2.21)	4.75 (4.66…4.79)	1.89 (1.8…2.02)

Table A4.3*: Event magnitude, probability ratio and change in intensity for 5-year return period for SST14x WMed for observational datasets and each model that passed the evaluation tests. (a) from pre-industrial climate to the present and (b) from the present to 2.8℃ above pre-industrial climate.*

		Preindustrial - Present (1.4˚C)		**Present - Future (2.8˚C)**	
Model / Observations	**Threshold for return period 1.5 yr**	**Probability ratio PR [-]**	**Change in intensity ΔI [˚C]**	**Probability ratio PR [-]**	**Change in intensity ΔI [˚C]**
ERA5SST	1.39˚C	954.67 (160.05…15797.92)	1.88 (1.51…2.28)		
OISST	1.23˚C	17324166.13 (78152.42…534798440895.5)	2.77 (2.03…3.57)		
OSTIA	1.09˚C	32839.37 (1392.6…433269805.47)	3.19 (2.14…4.43)		
CanESM5_r10i1p1f1	27.49˚C	242.79 (186.11…796.71)	1.49 (1.46…1.58)	1.5 (1.5…1.5)	1.61 (1.59…1.62)
CMCC-CM2-SR5_r1i1p1f1	28.14˚C	1116.86 (471.49…4103.79)	1.89 (1.7…1.99)	1.5 (1.5…1.5)	1.8 (1.71…1.86)
CNRM-CM6-1_r2i1p1f2	27.95˚C	26.92 (19.14…96.06)	1.32 (1.23…1.54)	1.5 (1.5…1.5)	1.45 (1.41…1.52)
CNRM-ESM2-1_r1i1p1f2	28.46˚C	93.58 (46.73…814.05)	1.41 (1.33…1.6)	1.5 (1.5…1.5)	1.49 (1.5…1.67)
GFDL-CM4_r1i1p1f1	27.54˚C	489.06 (179.05…1644.1)	1.81 (1.51…1.9)	1.5 (1.5…1.5)	1.68 (1.64…1.74)
HadGEM3-GC31-LL_r1i1p1f3	27.98˚C	144.92 (24.89…371.7)	1.73 (1.39…1.79)	1.5 (1.5…1.5)	1.54 (1.54…1.59)
NESM3_r1i1p1f1	28.25˚C	218.13 (87.69…2014.06)	2.2 (1.88…2.54)	1.5 (1.5…1.5)	2.09 (2.05…2.17)

NorESM2-MM_r1i1p1f1	27.31˚C	477.72 (219.73…2130.3)	1.9 (1.77…2.11)	1.5 (1.5…1.5)	2.13 (2.06…2.26)
UKESM1-0-LL_r1i1p1f2	28.07˚C	74.79 (102.53…469.7)	1.68 (1.72…1.92)	1.5 (1.5…1.5)	1.58 (1.52…1.61)

Table A4.4*: Event magnitude, probability ratio and change in intensity for 1.5-year return period for SST14x EMed for observational datasets and each model that passed the evaluation tests. (a) from pre-industrial climate to the present and (b) from the present to 2.8℃ above pre-industrial climate.*